CHALMERS
UNIVERSITY OF TECHNOLOGY

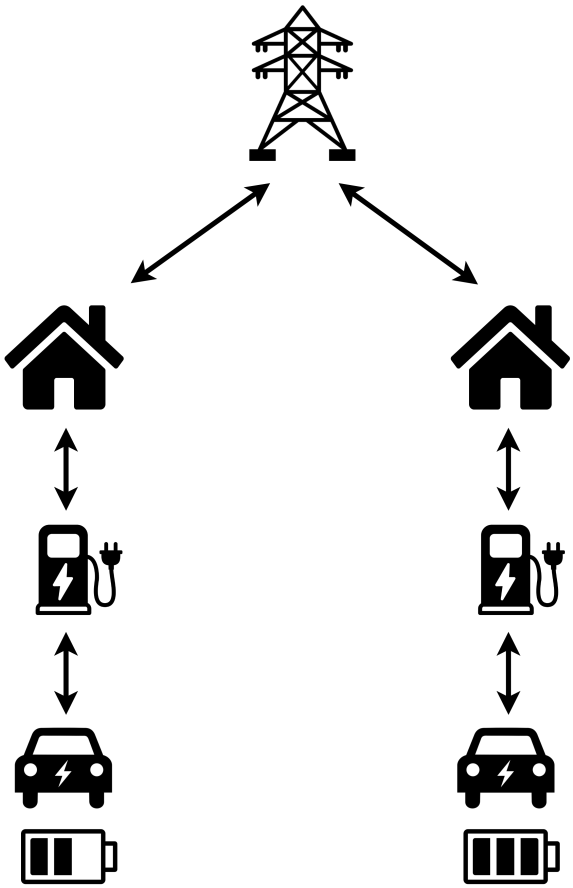

Vehicle-to-Everything Optimization Considering Battery Degradation

Master's Thesis in Data Science and AI & Engineering Mathematics and Computational Science

KALLE BJUREK
VICTOR HAGMAN

DEPARTMENT OF ELECTRICAL ENGINEERING

CHALMERS UNIVERSITY OF TECHNOLOGY
Gothenburg, Sweden 2022
www.chalmers.se

Master's thesis 2022

Vehicle-to-Everything Optimization Considering Battery Degradation

KALLE BJUREK
VICTOR HAGMAN

CHALMERS
UNIVERSITY OF TECHNOLOGY

Department of Electrical Engineering
Division of Systems and Control
Chalmers University of Technology
Gothenburg, Sweden 2022

Vehicle-to-Everything Optimization Considering Battery Degradation
KALLE BJUREK
VICTOR HAGMAN

Supervisor: Chih Feng Lee, Developer, Polestar
Supervisor: Yang Li, Researcher, Chalmers University of Technology
Examiner: Changfu Zou, Associate Professor, Chalmers University of Technology

Master's Thesis 2022
Department of Electrical Engineering
Division of Systems and Control
Chalmers University of Technology
SE-412 96 Gothenburg
Telephone +46 31 772 1000

Cover: Visualization of bidirectional power flows in a vehicle-to-grid setup.

Typeset in LaTeX
Printed by Chalmers Reproservice
Gothenburg, Sweden 2022

Vehicle-to-Everything Optimization Considering Battery Degradation
KALLE BJUREK
VICTOR HAGMAN
Department of Electrical Engineering
Chalmers University of Technology

Abstract

To curb climate change, the consensus is that fossil fuel-based electricity generation shall be replaced by renewable power generation, and combustion engine vehicles substituted by electric vehicles (EVs). However, due to the unpredictability of weather, an increased share of renewable power generation from weather-dependent sources reduces the production predictability. Furthermore, a higher market penetration of EVs imposes further challenges for the grid operators, particularly when a large number of EVs are charged simultaneously, creating peak power demand.

In this thesis, we investigate two services to alleviate the conundrum of weather-dependent renewable power generation and rising EV share, namely vehicle-to-home (V2H) and vehicle-to-grid (V2G). In both applications, EV batteries are used to store electrical energy for later dispatch using a bidirectional charger. Specifically, V2H reduces peak power demand, while V2G strategies offer frequency regulation services to the transmission system operators (TSOs).

As these services increase battery usage, there is a concern regarding premature battery degradation. We show that the increased battery degradation is an important operating cost affecting the profitability of the services, where it can account for up to 30.2% of the electricity cost savings in V2H.

Furthermore, a comparison between uncontrolled charging, smart charging, and V2H is conducted. Comparing uncontrolled charging and V2H, the results show that an EV owner in Sweden could potentially have saved between 13.3% and 35.9% of the household energy cost when the EV was plugged in during 2021.

Extending the idea of V2H in a single household, aggregated fleets of EVs are also studied. Smart charging is compared with both V2H and combinations of frequency regulation services. Examining four days in different seasons during 2021-2022, the results indicate that offering frequency regulation services yielded additional monetary savings between 87.4% and 307.3% compared with smart charging.

In conclusion, V2H and V2G demonstrate promising abilities to reduce energy costs while shifting high loads and regulating grid frequency, even when battery degradation is considered.

Keywords: electric vehicles, vehicle-to-home, vehicle-to-grid, frequency regulation, battery degradation, bidirectional charging, smart charging.

Acknowledgements

Firstly, we would like to send a big thank you to our Polestar supervisor Chih Feng Lee for showing great enthusiasm and encouragement throughout the thesis, as well as for supporting us with his expertise. We would also like to thank the members of the Charging and Energy team at Polestar R&D for providing important feedback during our work, and also for making us feel welcome in the Polestar HQ office.

Secondly, we would like to thank the Chalmers team consisting of our supervisor Yang Li and examiner Changfu Zou, for providing us with valuable feedback, knowledge, and support throughout our work with the thesis. The discussions have been of great help in the development of the thesis.

Last but not least, this thesis work would not have been possible without the support from our family and friends. Thank you for always being there for us.

Kalle Bjurek and Victor Hagman, Gothenburg, June 2022

List of Acronyms

Below is the list of acronyms that have been used throughout this thesis listed in alphabetical order:

BM	Bucket Model
DoD	Depth of Discharge
ECM	Equivalent Circuit Model
EV	Electric Vehicle
FCR	Frequency Containment Reserve
FCR-N	Frequency Containment Reserve Normal
FCR-D	Frequency Containment Reserve Disturbance
Li-ion	Lithium-ion
LSTM	Long Short-Term Memory
OCV	Open-Circuit Voltage
ReLU	Rectified Linear Unit
RMS	Root-Mean-Square
RMSE	Root-Mean-Square Error
SC	Smart Charging
SEI	Solid Electrolyte Interphase
SoC	State of Charge
TSO	Transmission System Operator
UC	Uncontrolled Charging
V2G	Vehicle-to-Grid
V2H	Vehicle-to-Home
V2X	Vehicle-to-Everything

Nomenclature

Below is the nomenclature of indices, sets, parameters, and variables that have been used throughout this thesis.

Indices/Sets

h ($\mathcal{H}$)	Index (set) of households
i ($\mathcal{I}$)	Index (set) of EVs
t ($\mathcal{T}$)	Index (set) of hourly time steps
t^{end}	Index of last entry in $\mathcal{T}$
t^{start}	Index of first entry in $\mathcal{T}$

Parameters

b^{age}	Initial battery age [days]
b^{cost}	Battery pack cost [SEK]
$b^{cap,kWh}$	Battery pack energy capacity [kWh]
$b^{cap,Ah}$	Battery cell charge capacity [Ah]
d^{dist}	Driving distance per year [km/year]
Δt	Time discretization step [h]
ΔSoC	Decrease in SoC due to driving [-]
E	Household energy consumption [kWh]
η	Charging/discharging efficiency [-]
G	Energy consumption per kilometer driven [kWh/km]
κ	Slope of linearized OCV in BM [V]
λ^{da}	Day-ahead market price for electricity [SEK/kWh]
λ^{r}	Regulation price [SEK/kWh]
λ^{b}	Regulation bid remuneration [SEK/kW]
N	Total number of battery cells in ECM [-]

N_p	Number of parallel strings of battery cells in ECM [-]
N_s	Number of series-connected battery cells in ECM [-]
OCV	Open-circuit voltage of battery cell [V]
P^{max}	Maximum charging power [kW]
P^{min}	Maximum discharging power [kW]
Q^{acc}	Accumulated battery cell throughput [Ah]
R	Series resistance in ECM [Ω]
R^{D2C}	Dispatch to contract ratio [-]
SoC^{ref}	Reference SoC level [-]
T^{acc}	Battery age [days]
T^{sim}	Simulation time [days]
θ	Battery temperature [K]
z^{init}	SoC at the start of the optimization horizon [-]
z^{end}	Minimum SoC at the end of the optimization horizon [-]
z^{max}	Maximum allowed SoC [-]
z^{min}	Minimum allowed SoC [-]

Variables

C^{lost}	Fraction of lost battery capacity [-]
d^{cal}	Calendar aging factor in BM [-]
d^{cyc}	Cycle aging factor in BM [-]
ΔDoD	Cycle depth [-]
I	Battery cell current [A]
λ^{deg}	Degradation cost of EV battery pack [SEK]
P^{bat}	EV battery power [kW]
P^{wall}	Wallbox power [kW]
Π^{bid}	Remuneration for offered regulation bids [SEK]
Π^{net}	Cost of household electricity, including EV charging [SEK]
Π^{reg}	Cost/income from bought/sold energy for FCR-N activation [SEK]
Q^{sim}	Battery cell throughput during simulation [Ah]
R^b	Regulation bid size [kW]
V	Battery cell voltage [V]
z	SoC [-]

Contents

List of Acronyms **ix**

Nomenclature **xi**

List of Figures **xv**

List of Tables **xvii**

1 Introduction **1**
1.1 Background . . . 1
1.2 Literature Review . . . 2
1.3 Aim . . . 3
1.4 Delimitations . . . 3
1.5 Thesis Outline . . . 4

2 Theory **5**
2.1 Electric Vehicle Batteries . . . 5
2.1.1 Degradation of Lithium-Ion Batteries . . . 7
2.1.2 Cell Configuration . . . 7
2.2 Frequency Regulation Markets . . . 9
2.2.1 Frequency Containment Reserve . . . 10

3 Battery Modeling **13**
3.1 Equivalent Circuit Model . . . 15
3.1.1 Degradation Modeling . . . 17
3.2 Bucket Model . . . 21
3.2.1 Degradation Modeling . . . 21
3.3 Differences in Cell Configuration . . . 22

4 Vehicle-to-Home **25**
4.1 Assumptions . . . 26
4.1.1 Time Discretization Step . . . 26
4.1.2 Charging Power and SoC Change . . . 26
4.1.3 Arrival and Departure Times . . . 26
4.1.4 Energy Consumption During Driving . . . 27
4.1.5 Parameter Values . . . 28
4.2 Creation of User Scenarios . . . 28

4.3 Equivalent Circuit Model 30
4.4 Bucket Model 32
4.5 Simulation Over Longer Time Periods 32
4.6 Household Energy Consumption Forecasting 34
4.7 Benchmark Models 35
4.8 Results 36
4.8.1 Equivalent Circuit Model 37
4.8.2 Comparison Between ECM and BM 41
4.9 Discussion 42

5 Vehicle-to-Grid **47**
5.1 Assumptions 48
5.1.1 Choice of Days 48
5.1.2 Individual EV Attributes 48
5.1.3 Prices and Activation 49
5.1.4 Household Energy Consumption 51
5.2 FCR-N 52
5.3 FCR-D up 53
5.4 Results 54
5.5 Discussion 56

6 Conclusion **59**

7 Future Work **61**

A Appendix **I**

List of Figures

2.1 Schematic figure of LCO cell. 6
2.2 Battery cells connected in series. 8
2.3 Battery cells connected in parallel. 8
2.4 Battery pack of parallel strings of series-connected cells. 9

3.1 Equivalent circuit model of 0th order. 15
3.2 OCV as a function of SoC with fourth-degree polynomial fit, and measured values. 16
3.3 10 year simulation of the battery degradation formula. 18
3.4 Comparison between the original formula for calendar aging and cycle aging versus new formulation. 20
3.5 Illustration of battery pack structure. 23

4.1 Visualization of power flow directions in V2H. 25
4.2 Example of smart charging within an optimization horizon. 35
4.3 Graphical visualization of costs related to each user scenario. 38
4.4 V2H charging power as seen from the wallbox. 39
4.5 Development of normalized capacity loss due to battery aging, for V2H. 40
4.6 Difference between the highest and lowest hourly electricity price within each optimization horizon of 2021. 43

5.1 Visualization of power flow directions for a fleet of EVs in a V2G solution. 47
5.2 Assumed activation of FCR-N for Days 1-4. 50
5.3 Energy consumption for households 1-3 during the selected days. . . . 51
5.4 Development of hourly electricity prices for Days 1-4. 57

A.1 V2H charging power as seen from the wallbox, short-distance drivers. II
A.2 V2H charging power as seen from the wallbox, average-distance drivers. III
A.3 V2H charging power as seen from the wallbox, long-distance drivers. . IV
A.4 Development of normalized capacity loss due to battery aging in V2H, short-distance drivers. V
A.5 Development of normalized capacity loss due to battery aging in V2H, average-distance drivers. VI
A.6 Development of normalized capacity loss due to battery aging in V2H, long-distance drivers. VII

List of Tables

2.1 Frequency statistics under 49.9 Hz for 2020 in the Nordic synchronous system. 11

3.1 Notation used in the battery models. 14
3.2 Battery cell specifications. 15
3.3 Fitted coefficients of fourth-degree polynomial for OCV estimation. . 16
3.4 Parameters in battery degradation equations. 17

4.1 Combinations of arrival and departure times and the number of hours in between. 27
4.2 Parameter values used in V2H. 28
4.3 Different user scenarios. 29
4.4 Structure of LSTM network in order from input to output. 34
4.5 Comparison of RMSEs between the LSTM and baseline. 34
4.6 Recapitulation of different user scenarios. 36
4.7 Comparisons of different user scenarios in the ECM, predicted household energy consumption. 37
4.8 Comparison between the ECM and BM for the V2H case using predicted household energy consumption. 41

5.1 Dates and times for optimization in the V2G case. 48
5.2 Truncated Gaussian distribution parameters used for sampling. 48
5.3 Comparisons of different days, using a fleet size of 1,000 EVs. 54
5.4 Comparisons of different days, using a fleet size of 500 EVs. 55

A.1 Comparisons of user scenarios in the ECM, actual household energy consumption. I

1
Introduction

1.1 Background

Global electricity consumption has been increasing steadily throughout the years, from 10,897 TWh in 1990 to 25,027 TWh in 2019, according to the International Energy Agency [1]. Simultaneously, their numbers show an increase in the share of renewable energy sources in power generation from 14.5% in 1990 to 23.2% in 2019. This development is an important step to reduce global warming.

However, production from renewable energy sources, such as wind power and photovoltaic systems, is weather dependent. This adds an uncertainty factor when the transmission system operators (TSOs) schedule energy production and consumption. An increasing share of electric vehicles (EVs) will impose further challenges for power production to meet power consumption. The sales market share of EVs has increased from 0.89% to 8.57% in just five years between 2016-2021, and EVs worldwide are estimated to consume over 30 TWh during 2022 according to [2]. The EV charging adds additional uncertainty to the scheduled power exchanges and creates peaks of power demand when several owners want to charge their EVs, usually in the afternoon or evening.

One way to avoid peak power demands is to implement smart charging that charges the EVs when the electricity price is low, usually corresponding to the period when power demand is low. Going further than the implementation of smart scheduling of charging, another strategy is to implement bidirectional charging and use the batteries of EVs to store energy for later use, using a so-called vehicle-to-everything (V2X) strategy. This could be to charge the EV battery when power demand is low, and save the cheaply bought energy for later usage in a household, a concept called vehicle-to-home (V2H), or to deliver power back to the grid when the demand is high or when energy production is lower than consumption. The latter concept is an example of vehicle-to-grid (V2G), which can be used to regulate the frequency of the grid. The V2X strategies also enable storing energy from renewable sources for later use.

1.2 Literature Review

A lot of research has been carried out in the V2X field. The concept of using EV batteries for delivering power to the grid is mentioned as early as 2001 by Kempton et al. [3]. The authors present different ways in which battery EVs, hybrid vehicles, and fuel cell vehicles can be used to generate revenue by supplying energy to the grid. The two ways mentioned to make a profit are to sell energy to the grid when demand and prices are high, and by providing ancillary services in the form of spinning reserves and regulation services.

Since the V2H and V2G concepts involve additional charging and discharging of batteries, these can lead to premature battery degradation. It is stated in [4] that battery degradation is composed of cycle aging and calendar aging, where cycle aging depends on the usage of the battery while calendar aging depends on its age and storage conditions, such as state of charge (SoC) and ambient temperature. Hence, this effect should be taken into account when developing strategies for V2H and V2G and analyzing financial benefits.

In [5], the authors specifically focus on quantifying the impact on EV battery degradation caused by normal driving and frequency regulation services on the Danish island of Bornholm. Their findings are that over a time horizon of 5 years, 6.1% battery degradation was caused by calendar aging, 0.8% by driving, while V2G frequency regulation resulted in 2% additional battery degradation.

In [6], a fleet of EVs offering frequency regulation services is examined. The results show a low potential to make monetary savings as a consequence of a high cost of battery degradation. However, this paper uses a high fixed cost for battery degradation, not dependent on cycle depth or historical usage of the EV battery. Moreover, the EV battery cost has decreased since the thesis was written, while the electricity prices have increased.

An optimal bidding strategy for an aggregator of EVs offering frequency regulation services is presented in [7]. The authors create synthetic data and use two-stage stochastic optimization to calculate potential profits in short-term electricity and regulation markets for unidirectional charging of EVs. Their work is built upon in [8], but the problem is implemented using real charging and driving data. Though, no bidirectional charging is examined in these papers.

There has been less focus on V2H in research. In cases where V2H has been considered, it often involves storing energy from a photovoltaic system in the EV battery to dispatch to the household at a later time, as in [9] and [10]. Moreover, these do not consider the impact on battery degradation.

To the best of the authors' knowledge, the field lacks research regarding V2H for a single household, without the inclusion of a photovoltaic system, while considering a dynamic battery degradation model accounting for the charging behavior and the

historical usage of the EV battery. Moreover, the thesis authors have also identified an absence of studies combining V2H with a community of EVs offering frequency regulation services through V2G.

1.3 Aim

The first thesis aim is to evaluate different scenarios of an EV utilizing V2H to make a saving on the household electricity cost while considering a dynamic cost of battery degradation. The second thesis aim is to quantify financial benefits for an aggregator of a fleet of EVs combining V2H and providing frequency regulation services through V2G, with battery degradation considered.

1.4 Delimitations

The thesis will be bounded by the following general delimitations:

- Day-ahead market prices for electricity, remuneration for procured bids, and regulation prices on an hourly basis are extracted for price region SE3 in Sweden where applicable. These prices are given in EUR. To convert the prices to SEK, a fixed exchange rate of 1 EUR = 10 SEK is used for simplicity.

- Households are assumed to have a variable electricity cost following the day-ahead market prices on an hourly basis.

- The EV battery energy capacity and charging power are chosen to correspond to the Polestar 2 Long range Single motor, with a battery energy capacity of 78 kWh and a maximum level 2 charging power of 11 kW.

- Each EV is assumed to be able to discharge with the same power to the wallbox as it can charge from the wallbox.

- The aggregator of EVs is assumed to fulfill all necessary prequalification steps to be able to provide frequency regulation services and is assumed to not cause any frequency imbalances. Moreover, all offered bids are assumed to be procured.

Additional scenario-specific delimitations and assumptions will be introduced continuously.

1.5 Thesis Outline

This introductory chapter will be followed by a theoretical chapter, providing a foundation to facilitate understanding of the thesis. Thereafter, a chapter describing the used battery models will be given. The battery modeling chapter will be followed by two separate chapters for V2H and V2G, presenting scenarios, results, and discussions separately. Lastly, the thesis conclusion will be summarized and suggestions for future work will be provided.

2
Theory

In this chapter, a foundation to facilitate understanding of the thesis will be given. It will start with a section describing EV batteries, how battery degradation happens, and how battery cells can be configured into a battery pack. Afterward, the Swedish frequency regulation market will be introduced, with a detailed focus on the products that will be used later in the thesis.

2.1 Electric Vehicle Batteries

The battery is a component of major importance in an EV, not least in terms of cost, as it can make up 1/3 of the total cost of the vehicle [11]. According to [12], the most important properties for describing such batteries are energy density, C-rate, lifetime, and cost. Energy density measures the energy capacity per volume unit (volumetric) or per weight unit (gravimetric), while the C-rate quantifies the maximum possible power output of the battery relative to its capacity. To improve such properties, batteries have undergone substantial development during the last years, and different cell chemistries have been deployed. Starting with hybrid EVs, a popular type of cell chemistry for many years was nickel-metal hydride (NiMH) [13]. For EVs, the current norm is lithium-ion (Li-ion) batteries. These batteries have higher energy density and lower self-discharge rate compared to NiMH, making them more suitable for EV applications [13].

To understand the degradation factors in Li-ion batteries, some basic information about the operating principle of a battery cell will be described. The reference used for this paragraph is [14], where the reader can find more detailed information. Three important components of a battery cell are the positive electrode (cathode), the negative electrode (anode), and the electrolyte. There may also be certain current collectors attached to the electrodes to facilitate the connection of the battery. Another component is the separator, which prevents electrons from moving between the two electrodes. In a charged battery cell, there will be a potential across the electrodes. When closing a circuit between the poles of a charged battery cell, the negative electrode will oxidize and release electrons to the external circuit. These electrons will be received by the positive electrode, a process which is called reduction. Simultaneously, positively charged ions will move through the electrolyte to the positive electrode. In rechargeable battery cells, this chemical process is reversible, and electrons and positively charged ions can move back from the positive electrode to the negative electrode. The charging process is induced by

feeding energy to the battery cell and causing a higher potential over the electrodes than its internal potential.

There are numerous types of materials used for the internal components of a battery cell that affect its characteristics. For instance, different types of materials used in the electrodes will yield different cell voltages. As an example, a NiMH battery cell has a positive electrode of nickel hydroxide ($Ni(OH)_2$) and a negative electrode of hydrogen absorbing alloy (MH) [15]. This configuration results in a voltage of about 1.2 V. On the other hand, Li-ion battery cells mostly use different forms of graphite for the negative electrode, while there exist several variants in the choice of material for the positive electrode. Some examples include lithium cobalt oxide (LCO), lithium nickel manganese cobalt oxide (NMC), and lithium iron phosphate (LFP). For these types of battery cells, the voltage is higher than NiMH. For instance, an NMC cell typically has a nominal voltage of 3.7 V [16]. Apart from the voltage, the selected type of lithium metal oxide used in the positive electrode also affects other characteristics of the cell. As an example, LFP cells have high C-rates but low energy densities, while NMC cells have low C-rates but high energy densities, when compared with other Li-ion variants [16].

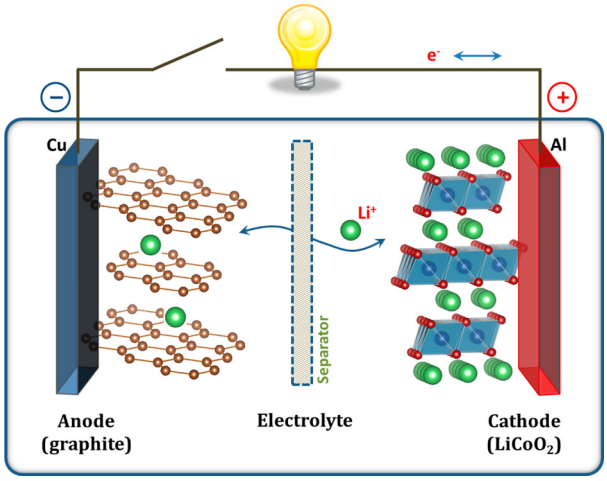

Figure 2.1: Schematic figure of LCO cell [17].[1]

Linking back to the description of the charge and discharge process of a battery cell, in Li-ion battery cells it is lithium atoms in the negative electrode that releases electrons upon discharge and transform into lithium ions. However, instead of forming new compounds in the electrodes through chemical reactions, the lithium will either be inserted into, or removed from, the material structure of the electrode. Thus, after releasing electrons, lithium ions will travel through the electrolyte to the opposite electrode where they will be integrated into the material. This process is shown in Figure 2.1, which depicts an LCO cell. The electrolyte in Li-ion battery cells is composed of a salt and a solvent [14].

[1]Reprinted with permission from J. B. Goodenough and K.-S. Park, "The Li-Ion Rechargeable Battery: A Perspective," Journal of the American Chemical Society, vol. 135, no. 4, pp. 1167–1176, 2013. Copyright 2013 American Chemical Society

2.1.1 Degradation of Lithium-Ion Batteries

One of the major causes of battery degradation is the build-up of a solid electrolyte interphase (SEI) layer on the graphite in the negative electrode. This is a result of a high reactivity between most of the common solvents in the electrolyte and the graphite in the positive electrode. This layer is formed directly during the first charge of the battery cell and acts as a protective layer for further reactions with the graphite. However, during the lifetime of the cell, the SEI layer tends to grow slowly, and will both increase the resistance of the cell and consume lithium, which lowers the capacity of the cell [14]. Also, when cycling the cell, the movement of lithium causes volume changes on the electrodes. This can cause stresses that propagate cracks on the electrode, and hence increase the surface exposed to the electrolyte. The increased surface will result in even more SEI formation [18].

The above-mentioned causes of degradation of Li-ion battery cells are some of the most prominent. The total degradation of a battery cell can be separated into the degradation that is caused by cycling the battery, denoted as cycle aging, and the degradation that is caused independent from cycling, which is denoted as calendar aging [19].

2.1.2 Cell Configuration

An EV battery pack consists of many battery cells configured in a certain structure to obtain desired battery pack specifications. For instance, the Polestar 2 battery voltage is 400 V, and it is obtained by arranging several cells with lower voltage in a certain structure to obtain the higher voltage. Another property of battery cells is charge capacity, which is often measured in ampere-seconds or ampere-hours (Ah), and measures what charge the battery can deliver. The capacity of a battery cell can also be stated as its energy capacity, measuring how much energy the battery cell can deliver, in watt-hours (Wh) or kilowatt-hours (kWh). As an example, the Polestar 2 Long Range battery pack has an energy capacity of 78 kWh, which is obtained by arranging several battery cells with lower capacity in a certain scheme.

When connecting multiple battery cells in series, the resulting battery pack voltage will be the sum of the voltages of the individual cells. The total charge capacity will however remain unchanged, as the current through all cells in a series connection will be the same. For instance, assuming that the charge capacity of one cell is 2 Ah, the charge capacity of the battery pack will be 2 Ah if all cells are connected in series. The energy capacity, on the other hand, will increase as the voltage increases. In Figure 2.2, an example battery pack is shown, where the individual cells are assumed to have a voltage of 3 V and a charge capacity of 2 Ah. The resulting voltage of the battery pack will hence be 9 V, the charge capacity 2 Ah and, the energy capacity $9\ \text{V} \cdot 2\ \text{Ah} = 18\ \text{Wh}$.

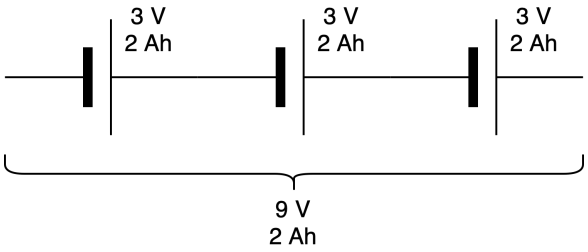

Figure 2.2: Battery cells connected in series.

By connecting cells in parallel, the charge capacity of the battery pack will be the sum of the individual charge capacities of the cells connected in parallel. The battery pack voltage will remain unchanged when cells are connected in parallel. An example battery pack is shown in Figure 2.3, having a voltage of 3 V and a charge capacity of 6 Ah. Note that the energy capacity of the battery pack is 18 Wh, which is the same as in Figure 2.2 where the cells were connected in series.

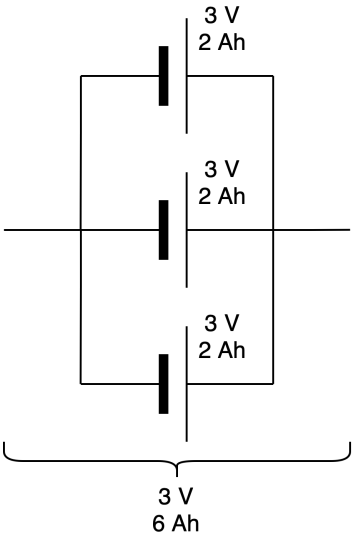

Figure 2.3: Battery cells connected in parallel.

Connecting strings of series-connected cells in parallel, a resulting example battery pack configuration can be seen in Figure 2.4. The energy capacity becomes 54 Wh, three times the energy capacity of the two previous examples.

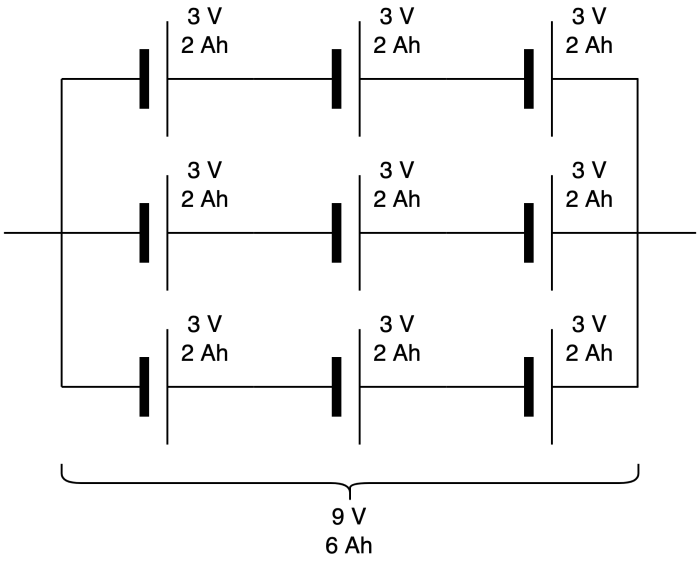

Figure 2.4: Battery pack of parallel strings of series-connected cells.

2.2 Frequency Regulation Markets

For the electric power system to work efficiently, there must be a balance between production and consumption of power. If there is a sudden deviation from the planned schedules of production and consumption, the frequency of the grid will deviate from the nominal frequency, which in Europe is 50 Hz [20]. A stable frequency is of utter importance since our electrical appliances are produced to work at this certain frequency, and a deviation can lead to non-working devices [21]. Furthermore, large frequency deviations will cause instability problems and can lead to failure of the system operation. If energy production is higher than consumption, the frequency of the grid will rise above the nominal value, and downregulation of the frequency is necessary, while if consumption is higher than production, the frequency will drop under the nominal value, and upregulation is required. Within a synchronous area, the grid is connected in an AC network, meaning that the frequency is the same everywhere in a synchronous system [22]. The Nordic synchronous system covers Sweden, Finland, Norway, and eastern Denmark [23].

The TSOs are responsible for maintaining the frequency of the grid. To their aid, they have different types of resources for regulating the frequency. These differ in terms of requirements, such as activation speed and endurance, and the requirements differ between countries. In Sweden, the TSO is Svenska Kraftnät, and the products available are Fast Frequency Reserve (FFR), Frequency Containment Reserve (FCR), automatic Frequency Restoration Reserve (aFRR), and manual Frequency Restoration Reserve (mFRR) [24]. These products are traded on markets where market participants can offer capacity of a product at a certain price, such that it can be procured by the TSO. There are also requirements on the minimum bid size, in terms of regulating capacity, of the products that can be offered on the

markets. While this might not be an issue for larger market players, it prevents small-scale actors such as individual households from participating in frequency regulation markets. An approach to circumvent this issue is to aggregate the capacity of many smaller units such that the combined capacity can be traded. A market actor consolidating capacities is called an aggregator [25]. Regardless of being an aggregator or not, all market participants must pass a prequalification process showing that the technical requirements for the specific product are met [26]. In the following subsection, the Swedish frequency regulation services relevant to this thesis will be described.

2.2.1 Frequency Containment Reserve

The Frequency Containment Reserve (FCR) stabilizes the frequency in case of deviations and is a vital part of regulating the frequency of the grid. The service is automatically activated if the frequency deviates inside the specified regulation region. The FCR is divided into two products, FCR-N where the N stands for normal operation, and FCR-D where D stands for disturbed operation. Note that the product specifications and numbers in the following subsections are specific for the Swedish market.

FCR-N

FCR-N is a product for frequency regulation in both up and down directions. It is symmetrical as the offered capacity has to be available for activation in both directions. The region for activation is between 49.90 Hz to 50.10 Hz, and the minimum bid size is 0.1 MW. The approximate volume requirement for Sweden is 240 MW. The product is activated linearly, with 100% activation of the bid at 50.10 Hz and -100% activation at 49.90 Hz, where negative activation implies upregulation. Regarding reaction time, 63% of the given activation must be made within 60 seconds of a deviation, and 100% within 3 minutes, while the activation endurance must be at least one hour [27].

FCR-D

FCR-D is a product offering frequency regulation only in one direction. Earlier, only the product for upregulation, FCR-D up, existed in Sweden. However in 2022, a product for downregulation, FCR-D down, was also introduced [28]. These services are automatically activated and stabilize the frequency in the event of a disturbance, defined as when the frequency is outside the standard range of 49.90 Hz to 50.10 Hz [29]. In this thesis, only FCR-D up will be considered since it is more applicable in a bidirectional charging setup than FCR-D down.

FCR-D up operates in the region between 49.50 Hz to 49.90 Hz and is activated linearly, with 100% activation if the frequency is 49.50 Hz and 0% activation if the frequency is 49.9 Hz. The minimum bid size is 0.1 MW and the volume requirement for Sweden is up to 580 MW. The required activation time is 50% within 5 seconds

and 100% within 30 seconds, and endurance should be at least 20 minutes [29].

Statistics for frequency deviations below 49.90 Hz in the Nordic synchronous system from Fingrid's frequency quality analysis for 2020 [30] are presented in Table 2.1.

Table 2.1: Frequency statistics under 49.90 Hz for 2020 in the Nordic synchronous system [30].

Frequency [Hz]	No. deviations	Max duration [s]	Avg. duration [s]
< 49.90	26,568	922.3	9.6
< 49.80	112	390.7	9.5
< 49.70	6	17.9	7.8
< 49.60	1	2.7	2.7
< 49.50	0	0	0

This implies that during 2020, FCR-D up was rarely activated more than 0-25%, corresponding to the frequency interval 49.90-49.80 Hz.

Bidding Procedure and Remuneration

Procurement of the FCR products takes place both two days (D-2) and one day (D-1) before delivery. The majority of the capacity is procured D-2 and the rest D-1. The bidding process is a closed auction, meaning that participants are unaware of each other's bids. The deadline for submitting bids D-2 is 15:00, and for D-1 it is 18:00 [31]. After the respective deadline, Svenska Kraftnät consolidates the bids, sorts them in ascending order, and accepts the bids with the lowest asking prices summing up to the total product volume requirement.

Procured bids for FCR-N capacity are reimbursed according to "pay-as-bid", while activation of capacity is priced according to the upregulation and downregulation prices on Nord Pool power exchange [27]. For upregulation, the activated energy is reimbursed according to the upregulation price, which is at least the day-ahead price. For downregulation, the activated energy is bought to the downregulation price, which at most equals the day-ahead price [32]. For FCR-D, procured bids are reimbursed according to "pay-as-bid", while there is no reimbursement or cost for activation [29].

3
Battery Modeling

In the following chapter, two battery models used to describe the dynamic behaviors of the EV battery pack will be introduced. These two models were inspired by the ones used in [33], with minor modifications to their formulations. Differences and corresponding motivations will be explained in the upcoming model definitions. The first model to be introduced is an equivalent circuit model (ECM), followed by a simpler bucket model (BM). The purpose of developing the BM was to simplify the ECM for usage in a large-scale V2G application in Chapter 5, to lower the computational complexity.

Table 3.1 introduces battery-related notation that will be used throughout the thesis in alphabetical order, including units where applicable. The battery temperature was assumed to be held constant by an external thermal management system at 298 K, corresponding to approximately 25°C.

Table 3.1: Notation used in the battery models.

Symbol		Definition	Unit
$b^{cap,Ah}$	:=	Battery cell charge capacity	Ah
$b^{cap,kWh}$	:=	Battery pack energy capacity	kWh
$C^{lost,ECM}$	:=	Fraction of lost battery cell capacity for ECM	-
$C^{lost,BM}$	:=	Fraction of lost battery pack capacity for BM	-
d^{cal}	:=	Calendar aging factor in BM	-
d^{cyc}	:=	Cycle aging factor in BM	-
ΔDoD	:=	Cycle depth	-
$I(t)$	:=	Battery cell current at time t	A
N	:=	Total number of battery cells in ECM	-
N_p	:=	Number of parallel strings of battery cells in ECM	-
N_s	:=	Number of series-connected battery cells in ECM	-
$OCV(z(t))$	:=	Open-circuit voltage at SoC level z at time t	V
$P(t)$	:=	Battery power at time t	W
Q^{acc}	:=	Accumulated battery cell throughput	Ah
Q^{sim}	:=	Battery cell throughput during simulation	Ah
R	:=	Series resistance in ECM	Ω
T^{acc}	:=	Battery age	days
T^{sim}	:=	Simulation time	days
θ	:=	Battery temperature	K
$V(t)$	:=	Battery voltage at time t	V
$z(t)$	:=	SoC at time t	-

3.1 Equivalent Circuit Model

The battery cell used for the ECM was a 18650 Li-ion battery from the producer Sanyo, model UR18650E. The cell is designed for automotive application and is composed of a carbon cathode and a $Li(NiMnCo)O_2$ anode [34]. Other cell specifications are given in Table 3.2.

Table 3.2: Battery cell specifications, from [34] unless other stated.

Nominal capacity	2.05 Ah
Nominal voltage	3.6 V
Lower voltage limit	2.5 V
Upper voltage limit	4.2 V
Internal resistance	0.0334 Ω [35]

A 0th-order ECM is used in this thesis. A visualization is given in Figure 3.1.

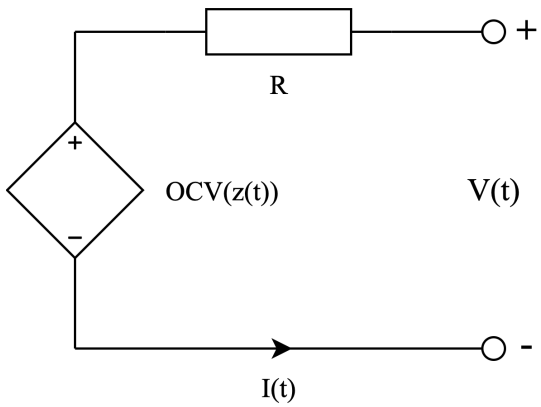

Figure 3.1: Equivalent circuit model of 0th order.

The control variable in this model is the battery cell current $I(t)$, where a positive current indicates that the battery is being charged, and a negative current indicates discharging of the battery. Equation (3.1) describes the relationship between the derivative of the SoC $z(t)$ as the current $I(t)$ divided by the battery charge capacity $b^{cap,Ah}$. Equation (3.2) limits the SoC $z(t)$ between 0, representing an empty battery, and 1, representing a fully charged battery.

$$\frac{dz(t)}{dt} = \frac{I(t)}{b^{cap,Ah}} \tag{3.1}$$

$$0 \leq z(t) \leq 1 \tag{3.2}$$

The battery cell voltage is given in (3.3) as the sum of the open-circuit voltage (OCV) for the given SoC level $z(t)$, and the product of the resistance R and current $I(t)$. Remembering that a negative current indicates discharging of the battery cell, the cell voltage drops during discharging.

$$V(t) = OCV(z(t)) + R \cdot I(t) \tag{3.3}$$

A polynomial for the OCV of the cell was fitted according to measured voltage values at different SoC levels, which are given in [34] for the selected battery cell. The coefficients obtained from the fit are shown in Table 3.3. The resulting fit can be observed in Figure 3.2.

Table 3.3: Fitted coefficients of fourth-degree polynomial for OCV estimation.

$\gamma_4 = -3.4599$
$\gamma_3 = 8.0326$
$\gamma_2 = -5.8485$
$\gamma_1 = 2.1021$
$\gamma_0 = 3.3324$

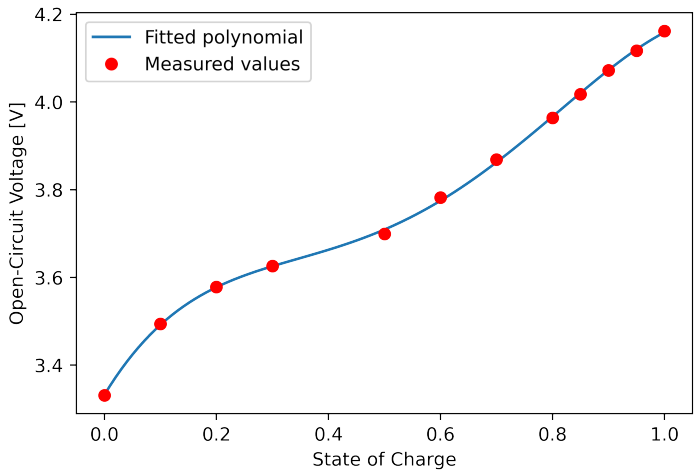

Figure 3.2: OCV as a function of SoC with fourth-degree polynomial fit, and measured values from [34].

The resulting polynomial has the form

$$OCV(z(t)) = \gamma_4 \cdot z(t)^4 + \gamma_3 \cdot z(t)^3 + \gamma_2 \cdot z(t)^2 + \gamma_1 \cdot z(t) + \gamma_0. \tag{3.4}$$

3.1.1 Degradation Modeling

The battery degradation in the ECM is defined as the lost capacity due to calendar aging and cycle aging. Schmalstieg et al. [4] provide a model for calculating the calendar aging and cycle aging separately on a battery cell level. The calendar aging depends on a factor α given by

$$\alpha(V(t), \theta) = (\epsilon_0 \cdot \bar{V} - \epsilon_1) \cdot \exp\left(-\frac{\epsilon_2}{\theta}\right), \tag{3.5}$$

where $\bar{V}$ is the average of $V(t)$ in the time horizon, θ is the battery temperature, and the values of ϵ_0, ϵ_1 and ϵ_2 are given in Table 3.4. The cycle aging depends on the factor β given by

$$\begin{aligned}\beta(V(t), z(t)) =& \zeta_0 \cdot (\varnothing V - \zeta_1)^2 + \zeta_2 \\ &+ \zeta_3 \cdot \Delta\text{DoD},\end{aligned} \tag{3.6}$$

where $\varnothing V$ is the root-mean-square (RMS) voltage $V(t)$ in the time horizon, and ζ_0, ζ_1, ζ_2, and ζ_3 can be found in Table 3.4.

Table 3.4: Parameters in battery degradation equations [4].

$\zeta_3 = 4.081 \cdot 10^{-3}$
$\zeta_2 = 7.600 \cdot 10^{-4}$
$\zeta_1 = 3.667$
$\zeta_0 = 7.348 \cdot 10^{-3}$
$\epsilon_2 = 6976$
$\epsilon_1 = 23.75 \cdot 10^{6}$
$\epsilon_0 = 7.543 \cdot 10^{6}$

A distinct definition of ΔDoD is not given in the original formulation by Schmalstieg et al. [4], hence in this thesis, ΔDoD was approximated as in [33], such that

$$\Delta\text{DoD} = 2 \cdot \frac{\int |\bar{z} - z(t)|\, dt}{|\mathcal{T}|}, \tag{3.7}$$

where $\bar{z}$ is the average SoC over the time horizon with length $|\mathcal{T}|$, and $z(t)$ is the SoC at time t.

The fraction of lost battery cell capacity relative to the initial battery cell capacity is then, according to [4], obtained by

$$C^{lost} = \alpha(V(t), \theta) \cdot (T^{acc})^{0.75} + \beta(V(t), z(t)) \cdot \sqrt{Q^{acc}}, \tag{3.8}$$

where T^{acc} is the age of the battery cell in days, and Q^{acc} is the total battery cell throughput during its lifetime in ampere-hours.

Figure 3.3 depicts an example development of the calendar aging and cycle aging over a simulation horizon of 10 years using the following assumptions:

- The battery cell throughput was caused by a normal driving pattern of 30 km/day and the corresponding daily charging.
- The battery temperature was held constant at 298 K.
- ΔDoD was set according to the daily SoC decrease due to driving.
- The mean voltage and root mean square voltage was set to the voltage at 50% SoC, calculated using the OCV curve (3.4).

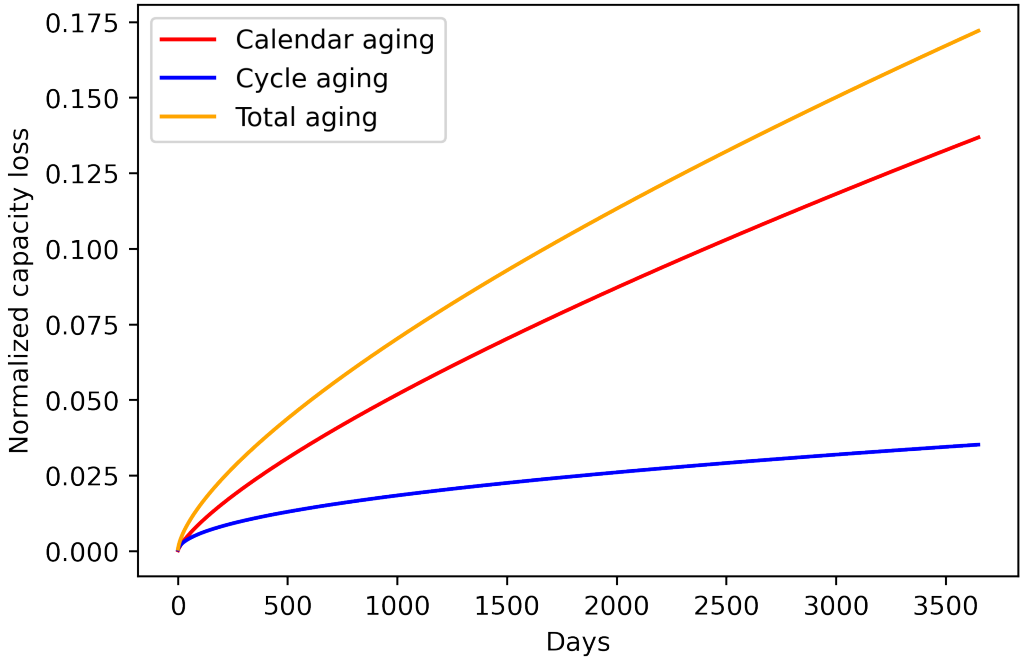

Figure 3.3: 10 year simulation of the battery degradation formula (3.8).

For practical applications, it is desirable to get the additional degradation caused by a specific usage pattern during one single time period, given the historical operation of the battery cell. Thus, given the age and historical throughput of the battery cell, the added degradation during a specific time period can be approximated using a Taylor series expansion. As a brief introduction, a Taylor series expansion can be used to approximate the value of a function f at a given point x and the derivatives of the function at an adjacent point a.

$$f(x) = f(a) + f'(a) \cdot (x-a) + \frac{f''(a)}{2!} \cdot (x-a)^2 + \frac{f'''(a)}{3!} \cdot (x-a)^3 + ... \tag{3.9}$$

To avoid adding unnecessary complexity to the upcoming optimization problem formulations in Chapters 4 and 5, it was decided that the first-order Taylor series expansion of the function was sufficient, i.e., to use the tangent to approximate the function value. This was done both for the calendar aging and the cycle aging. Starting with the calendar aging, replacing x in (3.9) with the sum of the time T^{acc} up until day $d-1$ and the simulation time T^{sim} of day d, a with the time T^{acc} up until day $d-1$, and $f(a) = (T^{acc})^{0.75}$ gives

$$\begin{aligned} f(T^{acc} + T^{sim}) &\approx (T^{acc})^{0.75} + 0.75 \cdot \frac{1}{(T^{acc})^{0.25}} \cdot ((T^{acc} + T^{sim}) - T^{acc}) \\ &= (T^{acc})^{0.75} + 0.75 \cdot \frac{T^{sim}}{(T^{acc})^{0.25}}. \end{aligned} \tag{3.10}$$

This implies that the capacity loss due to calendar aging during day d is a factor of

$$\begin{aligned} f(T^{acc} + T^{sim}) - f(T^{acc}) &\approx (T^{acc})^{0.75} + 0.75 \cdot \frac{T^{sim}}{(T^{acc})^{0.25}} - (T^{acc})^{0.75} \\ &= 0.75 \cdot \frac{T^{sim}}{(T^{acc})^{0.25}}. \end{aligned} \tag{3.11}$$

Combining the derived time factor with the function $\alpha(V(t), \theta)$ defined in (3.5), the capacity loss due to calendar aging during day d is approximately

$$\alpha(V(t), \theta) \cdot 0.75 \cdot \frac{T^{sim}}{(T^{acc})^{0.25}}. \tag{3.12}$$

Similarly, for the cycle aging formula, replacing x in (3.9) with the sum of the accumulated throughput Q^{acc} up until day $d-1$ and the throughput Q^{sim} for day d, a with the accumulated throughput Q^{acc} up until day $d-1$, and $f(Q^{acc}) = \sqrt{Q^{acc}}$ gives

$$\begin{aligned} f(Q^{acc} + Q^{sim}) &\approx \sqrt{Q^{acc}} + 0.5 \cdot \frac{1}{\sqrt{Q^{acc}}} \cdot ((Q^{acc} + Q^{sim}) - Q^{acc}) \\ &= \sqrt{Q^{acc}} + 0.5 \cdot \frac{Q^{sim}}{\sqrt{Q^{acc}}}. \end{aligned} \tag{3.13}$$

This implies that the added cycle aging during day d is a factor of

$$\begin{aligned} f(Q^{acc} + Q^{sim}) - f(Q^{acc}) &\approx \sqrt{Q^{acc}} + 0.5 \cdot \frac{Q^{sim}}{\sqrt{Q^{acc}}} - \sqrt{Q^{acc}} \\ &= 0.5 \cdot \frac{Q^{sim}}{\sqrt{Q^{acc}}}. \end{aligned} \tag{3.14}$$

Combining this throughput factor with the function $\beta(V(t), z(t))$ defined by (3.6), the capacity loss due to cycle aging during day d is approximately

$$\beta(V(t), z(t)) \cdot 0.5 \cdot \frac{Q^{sim}}{\sqrt{Q^{acc}}}. \tag{3.15}$$

In summary, the expression for the total fraction of lost capacity during one time horizon is

$$C^{lost,ECM} = \alpha(V(t),\theta) \cdot 0.75 \cdot \frac{T^{sim}}{(T^{acc})^{0.25}} + \beta(V(t),z(t)) \cdot 0.5 \cdot \frac{Q^{sim}}{\sqrt{Q^{acc}}}, \tag{3.16}$$

where, once again, T^{acc} is the age of the battery cell in days and Q^{acc} is the accumulated throughput of the battery cell in ampere-hours, both up until the start of the time horizon. T^{sim} is the length of the time horizon in days, and Q^{sim} is the battery throughput during the time horizon. The calendar aging function α was calculated according to (3.5) using the mean voltage over the time horizon, and β was calculated according to (3.6) using the RMS voltage and ΔDoD during the time horizon.

A visual comparison between the two formulas (3.8) and (3.16) is given in Figure 3.4 using the same assumptions as to produce Figure 3.3, but with a simulation period of only the first two years.

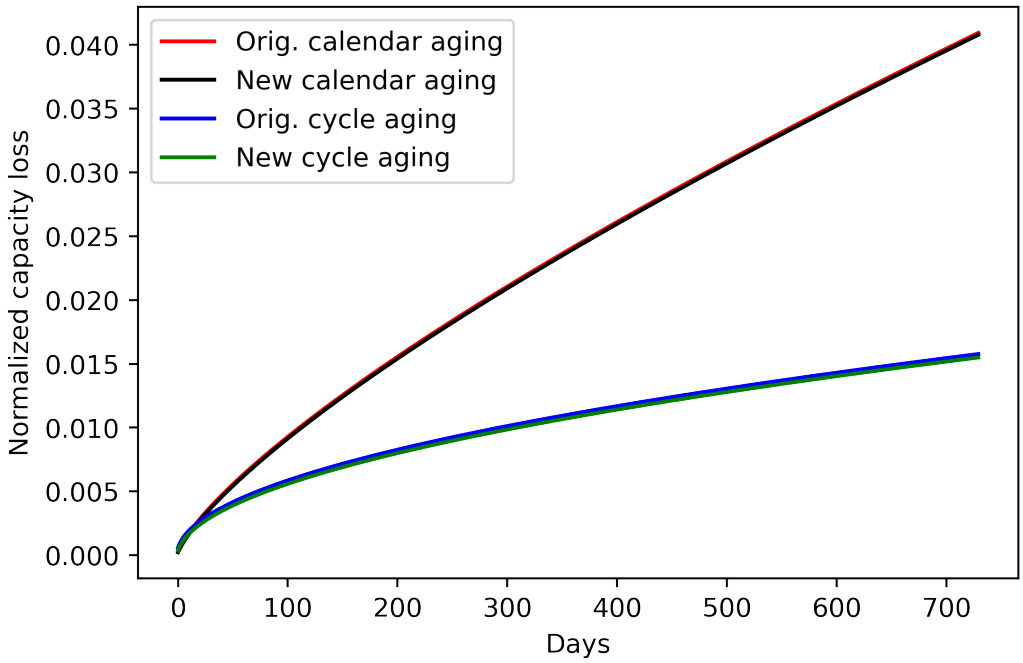

Figure 3.4: Comparison between the original formula for calendar aging and cycle aging (3.8) versus the new one (3.16).

The key with the new formulation compared to the original formulation is, as previously mentioned, that it can highlight short-term degradation effects, while the original formulation only accounts for long-term behavior.

3.2 Bucket Model

The BM is a simple battery model, also known as an energy reservoir model. As opposed to the ECM, the BM models the battery on a pack level and the control variable is the battery power. Equation (3.17) describes the relationship between the derivative of the SoC $z(t)$ as the battery power $P(t)$ divided by the battery energy capacity $b^{cap,kWh}$. Note that $b^{cap,kWh}$ is given on a battery pack level. Equation (3.18) describes that the SoC is limited between 0 and 1.

$$\frac{dz(t)}{dt} = \frac{P(t)}{b^{cap,kWh}} \tag{3.17}$$

$$0 \leq z(t) \leq 1 \tag{3.18}$$

In this model, there are no further restrictions except for limits on the battery power $P(t)$.

3.2.1 Degradation Modeling

In [33], the battery degradation in the BM was formulated as the fraction of lost capacity per power throughput, given by a degradation constant d^c, multiplied by the integral of the battery power as

$$d^c \cdot \int |P(t)| dt,$$

where d^c was calculated assuming that the battery reached its end-of-life after 8000 cycles.

In this thesis, the battery degradation was instead calculated to match the battery degradation of the ECM. Hence, the battery degradation in the BM, $C^{lost,BM}$, was formulated as the sum of capacity loss due to calendar aging, d^{cal}, and cycle aging, d^{cyc}.

$$C^{lost,BM} = d^{cal} + d^{cyc} \tag{3.19}$$

Even though the BM does not include any voltage variable, it was still of interest to create a similar calendar aging effect as in the ECM. To make the BM calendar aging function linear, the OCV parameterization described in (3.4) was linearized. The minimum voltage V^{min} was calculated using the polynomial at 0% SoC, while κ was calculated as

$$\kappa = \frac{\Delta OCV}{\Delta z} = \frac{OCV(1) - OCV(0)}{1 - 0} = 0.8263 \text{ V}.$$

Using V^{min} and κ, a linear relationship for the mean voltage was approximated by

$$\hat{\bar{V}} = V^{min} + \kappa \cdot \bar{z},$$

where $\bar{z}$ is the average SoC. Hence, the calendar aging effect in the BM could be expressed as

$$d^{cal} = \alpha(\bar{\hat{V}}, \theta) \cdot 0.75 \cdot \frac{T^{sim}}{(T^{acc})^{0.25}}, \tag{3.20}$$

where θ, once again, was set at a fixed temperature of 298 K.

Furthermore, the lost capacity due to cycle aging in the BM is

$$d^{cyc} = \beta(\hat{V}, \hat{z}) \cdot 0.5 \cdot \frac{Q^{sim}}{\sqrt{Q^{acc}}}. \tag{3.21}$$

In the formulation above, $\hat{V}$ and $\hat{z}$ are assumed values and not functions of time as in the ECM. $\hat{V}$ was set to the voltage corresponding to 50% SoC of the battery cell in the ECM. In the β function, $\hat{z}$ is used for estimating the cycle depth ΔDoD. In the BM, ΔDoD was constructed to reflect the cycle depth obtained from a comparable simulation of the ECM. This is explained in Section 4.5.

As the ECM models the battery on a cell level, the throughput Q^{sim} and Q^{acc} reflect the throughput of a single cell. However, as the BM models the battery on a pack level, the throughput had to be converted to cell level to match the degradation formulation in the ECM.

$$Q^{sim} = \frac{\int |P(t)|dt}{b^{cap,kWh}} \cdot b^{cap,Ah}$$

The historical throughput of the battery, Q^{acc}, was converted likewise.

3.3 Differences in Cell Configuration

As previously mentioned, a key difference between the ECM and the BM is that the ECM is given on a battery cell level, while the BM is given on a battery pack level. This implies that the battery in the BM is modeled as one big cell, while the ECM consists of several smaller cells with specifications given in Table 3.2. For simplification, the behavior and degradation of all battery cells are assumed to be homogeneous.

To reach the energy capacity of the Polestar 2 Long range Single motor of 78 kWh and the nominal battery pack voltage of 400 V, several battery cells had to be connected in a scheme in the ECM. The cell configuration was made assuming the cell voltage at 50% SoC, which was calculated using the fitted OCV coefficients in equation (3.4), resulting in a voltage of 3.7091 V. Therefore, to reach a nominal battery pack voltage of 400 V, the number of cells connected in series N_s was set to

$$N_s = \frac{400 \text{ V}}{3.7091 \text{ V}} \approx 108 \text{ cells in series.}$$

To calculate the number of parallel-connected strings N_p, the energy capacity of the full battery pack in kilowatt-hours was used, and the nominal charge capacity of a single cell in ampere-hours.

$$N_p = \frac{78000 \text{ Wh}}{400 \text{ V}} \cdot \frac{1}{2.05 \text{ Ah}} \approx 95 \text{ strings in parallel}$$

Multiplying these numbers, the ECM battery pack has a total number of cells N according to

$$N = N_s \cdot N_p = 108 \cdot 95 = 10,260.$$

The resulting structure of the battery pack is given in Figure 3.5.

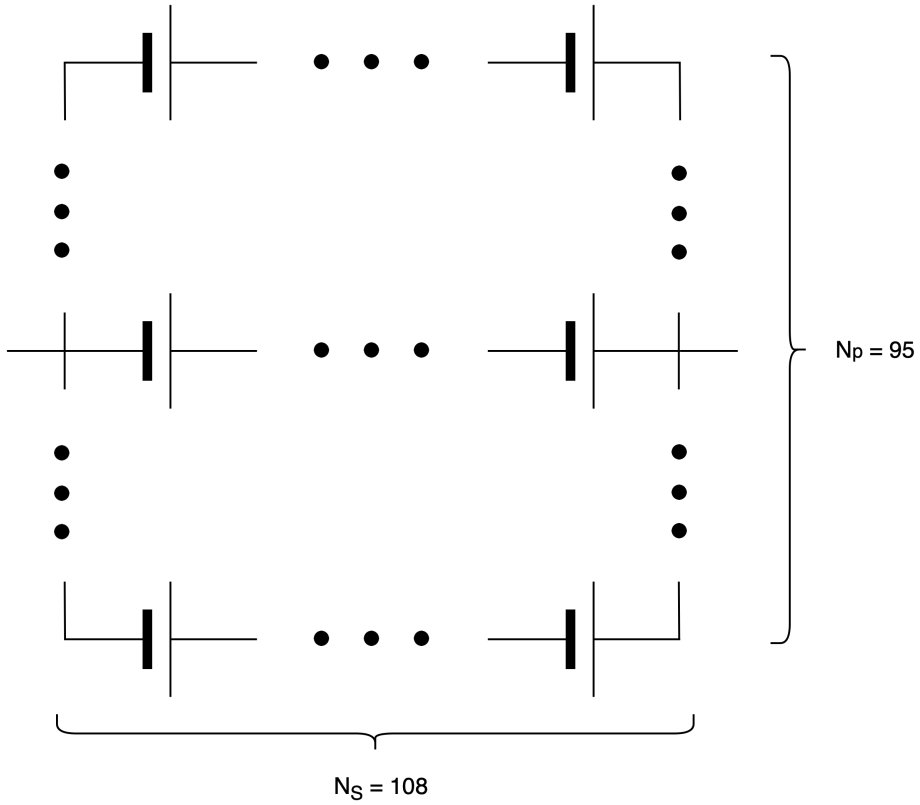

Figure 3.5: Illustration of battery pack structure.

Note that the battery cell used in this thesis is different from the battery cell used in the Polestar 2 Long range Single motor. Hence, the resulting configuration is fictional and does not reflect the actual Polestar 2 Long range Single motor battery pack configuration.

4
Vehicle-to-Home

In the V2H problem formulation, the battery models described in Chapter 3 were incorporated into optimization problem setups with the objective to reduce the electricity cost of a single household, while also considering the cost of increased battery degradation. The EV battery was used to store energy when the electricity prices were low and supply the energy to the household when the electricity prices were high. A schematic view of a V2H setup is given in Figure 4.1, where having both an EV and a charger allowing for bidirectional charging is necessary.

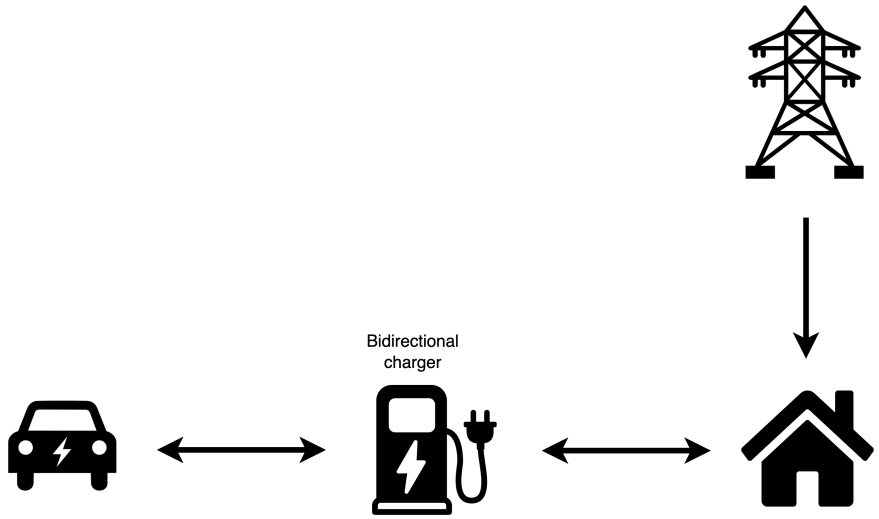

Figure 4.1: Visualization of power flow directions in V2H.

One frequently used reformulation in the upcoming optimization problem setups is the introduction of a new variable to produce an absolute value. If one wants to use an absolute value for a variable A, i.e., requests an $|A|$, this is formulated in code by introducing a new variable A^{abs} according to

$$A \leq A^{abs} \tag{4.1}$$
$$-A \leq A^{abs}. \tag{4.2}$$

A^{abs} is then equal to, or larger than, $|A|$. An important detail is that the optimization problem solver can choose the absolute value variable arbitrarily large to minimize or maximize the objective. Therefore, it can be necessary to penalize large values of the variable A^{abs} in the objective, depending on the spe-

cific problem formulation. To reduce the number of constraints in the following sections, an absolute value variable is written solely as $|A|$, but it is achieved in code by the introduction of the variable A^{abs} and the two constraints (4.1) and (4.2).

The optimization problems in this chapter were modeled using the open-source optimization library Pyomo in Python [36], [37]. Moreover, the open-source solver IPOPT [38] was chosen for solving the nonlinear optimization problems.

4.1 Assumptions

First, some general assumptions had to be made to set up the optimization problems. These will be given with motivations in the following subsections.

4.1.1 Time Discretization Step

When converting continuous time to discrete time, the time discretization step had to be chosen. The household energy consumption data used in the thesis was given on an hourly basis, as the total energy consumed during the specific hour. Therefore, a time discretization step of less than one hour would not add value since the hourly household energy consumption only would have been split into equal parts for each shorter time interval. Moreover, the day-ahead prices for electricity are also given on an hourly basis, adding an argument as to why a shorter time discretization step would not add value. Subsequently, the time discretization step was chosen to be 1 hour.

4.1.2 Charging Power and SoC Change

An assumption connected to, and caused by, the choice of time discretization step was that the charging power during a specific hour t was assumed to be constant throughout the whole hour t, i.e. constant in the interval $[t,\ t+1)$. Consequently, the resulting change in SoC due to the charging behavior during hour t was seen in the SoC level at hour $t+1$. Hence, the SoC also changed at the hour of departure from the household.

4.1.3 Arrival and Departure Times

To get the optimization time horizon for each day, assumptions were made regarding the arrival time and departure time of the EV. The assumptions were that the EV arrived at the household at 17:00 and left the household at 8:00 the next day during workdays, while it arrived at the household at 15:00 and left at 10:00 the next day on weekends. All weekday combinations are summarized in Table 4.1, including the number of hours between the two timestamps.

Table 4.1: Combinations of arrival and departure times and the number of hours in between.

Weekday combination	Arrival time	Departure time	Hours
Monday-Tuesday	17:00	8:00	15
Tuesday-Wednesday	17:00	8:00	15
Wednesday-Thursday	17:00	8:00	15
Thursday-Friday	17:00	8:00	15
Friday-Saturday	17:00	10:00	17
Saturday-Sunday	15:00	10:00	19
Sunday-Monday	15:00	8:00	17

The year chosen for simulation was 2021. Hence, the first optimization horizon was between 17:00 January 1st and 10:00 January 2nd, since January 2nd was a Saturday. The last optimization horizon was between 17:00 December 30th and 8:00 December 31st, implying that the optimization was run 364 times. Using the combinations from Table 4.1, the EV was assumed to be plugged-in during 5,772 hours between 17:00 January 1st and 8:00 December 31st, out of the total 8,727 hours between the two timestamps.

4.1.4 Energy Consumption During Driving

Another necessary assumption was the EV energy consumption per kilometer driven, as this was used to calculate the decrease in SoC caused by driving. The Polestar 2 Long range Single motor has an energy consumption of 0.186 kWh/km under WLTP testing conditions according to [39], where the higher value in the table was used since the WLTP driving cycle has relatively favorable conditions.

4.1.5 Parameter Values

The parameter values used in the optimization problems are presented in Table 4.2.

Table 4.2: Parameter values used in V2H.

Parameter		Value	Unit
Δt	$\leftarrow$	1	h
η	$\leftarrow$	0.92	-
z^{min}	$\leftarrow$	0.1	-
z^{max}	$\leftarrow$	0.9	-
P^{min}	$\leftarrow$	-11	kW
P^{max}	$\leftarrow$	11	kW
$b^{cap,Ah}$	$\leftarrow$	2.05	Ah
$b^{cap,kWh}$	$\leftarrow$	78	kWh
b^{cost}	$\leftarrow$	96,174	SEK
G	$\leftarrow$	0.186	kWh/km
SoC^{ref}	$\leftarrow$	0.5	-

The motivation of the time discretization step Δt was given in Section 4.1.1. The efficiency in both charging and discharging direction η was set to the square root of the round-trip efficiency reported in [40] for an EV with an on-board AC/DC inverter used for bidirectional charging. The SoC limits z^{min} and z^{max} were set to 0.1 and 0.9, respectively. The lower limit was chosen as a precaution to always have a small energy buffer, while the upper limit was chosen to approximately correspond to the proposed end of charge voltage for the battery cell used in the ECM. P^{min} and P^{max} were set to the negative and positive values of the Polestar 2 Long range Single motor maximum level 2 charging power of 11 kW, respectively. $b^{cap,Ah}$ was set to the battery cell charge capacity, and $b^{cap,kWh}$ to the battery pack energy capacity of 78 kWh. The battery cost was calculated using a Li-ion battery pack cost of 137 USD/kWh in 2020 according to [41] and a fixed exchange rate of 1 USD = 9 SEK. This resulted in the battery cost $b^{cost} = 137$ USD/kWh $\cdot 78$ kWh $\cdot 9$ SEK/USD $=$ 96,174 SEK. The energy consumption per kilometer driven, G, was set to 0.186 kWh/km, as discussed in Section 4.1.4. The reference SoC that the EV at least should be charged to each day, SoC^{ref}, was set to 50%.

4.2 Creation of User Scenarios

The potential to profit from a V2H strategy is dependent on several factors, such as accumulated battery throughput and battery age. The more the battery has been cycled before due to driving and charging, the less additional capacity loss will be induced by V2H operation, as can be inferred from Figure 3.3. To compare scenarios with different historical EV usages, assumptions were made on driving distance per year and the battery age. From these assumptions it was possible to calculate the accumulated throughput on a cell level due to earlier driving. The formula used to calculate the historical accumulated throughput Q^{acc} is

$$Q^{acc} = 2 \cdot \frac{b^{age} \cdot \frac{d^{dist}}{365} \cdot G}{b^{cap,kWh}} \cdot b^{cap,Ah}, \tag{4.3}$$

where values of G, $b^{cap,kWh}$, and $b^{cap,Ah}$ were given in Table 4.2, while the driving distance per year, d^{dist}, and the battery age in days, b^{age}, are given as input parameters from Table 4.3 to calculate Q^{acc}. The expression was multiplied by 2 to include the historical throughput due to EV charging.

Table 4.3: Different user scenarios.

	d^{dist} [km]	b^{age} [days]
User 1	3,650	30
User 2	3,650	365
User 3	3,650	1,095
User 4	11,120	30
User 5	11,120	365
User 6	11,120	1,095
User 7	36,500	30
User 8	36,500	365
User 9	36,500	1,095

The shortest driving distance of 3,650 km per year was set according to a driving behavior of 10 km per day. The driving distance of 11,120 km per year was set according to the mean driving distance in Sweden during 2021 [42]. The last driving distance of 36,500 km per year was set according to a long-distance driver driving 100 km per day. The chosen battery ages were set to 1 month (30 days), 1 year (365 days), and 3 years (1,095 days).

In a similar way, the daily SoC decrease due to driving, denoted ΔSoC, was calculated as

$$\Delta\text{SoC} = \frac{\frac{d^{dist}}{365} \cdot G}{b^{cap,kWh}}. \tag{4.4}$$

This formula was used for the different user scenarios to calculate the SoC level of the EV when returning to the household after driving.

4.3 Equivalent Circuit Model

Using the ECM to model the battery cell dynamics and degradation, the V2H optimization problem was set up as a nonlinear program according to

$$\min \quad \Pi^{net,ECM} + \lambda^{deg,ECM} \tag{4.5}$$

$$\text{s.t.} \quad \Pi^{net,ECM} = \sum_t \left[\lambda_t^{da} \cdot (E_t + P_t^{wall} \cdot \Delta t)\right] \tag{4.6}$$

$$z_{t+1} = \frac{I_t}{b^{cap,Ah}} \Delta t + z_t \qquad \forall \quad t \tag{4.7}$$

$$P^{min} \leq P_t^{wall} \leq P^{max} \qquad \forall \quad t \tag{4.8}$$

$$z^{min} \leq z_t \leq z^{max} \qquad \forall \quad t \tag{4.9}$$

$$z_{t^{start}} = z^{init} \tag{4.10}$$

$$z_{t^{end}+1} \geq z^{end} \tag{4.11}$$

$$P_t^{wall} \cdot \Delta t \geq -E_t \qquad \forall \quad t \tag{4.12}$$

$$P_t^{wall} = P_t^{bat} + (1-\eta) \cdot |P_t^{bat}| \qquad \forall \quad t \tag{4.13}$$

$$OCV_t = \gamma_4 \cdot z_t^4 + \gamma_3 \cdot z_t^3 + \gamma_2 \cdot z_t^2 + \gamma_1 \cdot z_t + \gamma_0 \qquad \forall \quad t \tag{4.14}$$

$$V_t = OCV_t + R \cdot I_t \qquad \forall \quad t \tag{4.15}$$

$$P_t^{bat} = N \cdot V_t \cdot I_t \cdot 10^{-3} \qquad \forall \quad t \tag{4.16}$$

$$\lambda^{deg,ECM} = C^{lost,ECM} \cdot b^{cost} \tag{4.17}$$

The objective function (4.5) minimizes the sum of the total household electricity cost, $\Pi^{net,ECM}$, and the cost of battery degradation, $\lambda^{deg,ECM}$. $\Pi^{net,ECM}$ is set in (4.6) as the sum over all hours t of the day-ahead price, λ_t^{da}, multiplied by the sum of the household energy consumption, E_t, and the energy exchanged between the EV and the wallbox, $P_t^{wall} \cdot \Delta t$, where Δt is included to convert power to energy. Constraint (4.7) is a discretization of the expression for SoC change in the ECM, as described in (3.1). The power limits as seen from the wallbox are determined by (4.8). The SoC limits are set in (4.9). The start and end SoC levels are set in (4.10) and (4.11), respectively, where the inequality in (4.11) allows the EV to leave with a higher SoC than demanded. The maximum energy dispatched from the EV to the household is limited to the household energy consumption by (4.12), ensuring that energy from the EV cannot be delivered to the grid. The relationship between P_t^{wall} and P_t^{bat} is set in (4.13). A full derivation of this constraint is given in the next paragraph. Furthermore, the parametrization of the OCV curve, as introduced in (3.4), is expressed in constraint (4.14). The battery cell voltage, V_t, is set in constraint (4.15) as the sum of the OCV and the voltage over the resistance R. (4.16) expresses the battery pack power as the product of the number of cells N and the battery cell power, converted from Wh to kWh. (4.17) describes the cost of battery degradation as a product of the lost battery capacity as given in (3.16) and the cost of a new battery.

Derivation of constraint (4.13)

P_t^{wall} is the power as seen from the wallbox, i.e., before losses. Both when charging and discharging the EV, there will be losses, such as transformation losses between AC and DC. The relationship between the battery power P_t^{bat} and the wallbox power P_t^{wall} is described as

$$P_t^{bat} = \begin{cases} \eta \cdot P_t^{wall} & \text{if } P_t^{wall} \geq 0 \\ \frac{1}{\eta} \cdot P_t^{wall} & \text{if } P_t^{wall} < 0 \end{cases} \quad \forall \quad t \in \mathcal{T} \tag{4.18}$$

This implies that both when charging and discharging the EV, the battery power is smaller than the wallbox power, as the efficiency $\eta \leq 1$, indicating that there are losses in the bidirectional flow between the EV battery and the wallbox. The expression in (4.18) can be rewritten as

$$P_t^{wall} = \begin{cases} (1-(1-\eta))^{-1} \cdot P_t^{bat} & \text{if } P_t^{bat} \geq 0 \\ 1-(1-\eta) \cdot P_t^{bat} & \text{if } P_t^{bat} < 0 \end{cases} \quad \forall \quad t \in \mathcal{T}$$

$$\{\text{Replace } (1-\eta) \text{ with } \alpha\} \Rightarrow P_t^{wall} = \begin{cases} (1-\alpha)^{-1} \cdot P_t^{bat} & \text{if } P_t^{bat} \geq 0 \\ (1-\alpha) \cdot P_t^{bat} & \text{if } P_t^{bat} < 0 \end{cases}$$

Then, the factor $(1-\alpha)^{-1}$ can be expressed using a function $f(x)$ as

$$f(x) = (1+x)^n,$$

such that

$$f(-\alpha) = (1-\alpha)^{-1}, \quad \text{when } n = -1$$

Expressing this as a Maclaurin series and approximating it with the first order yields

$$\begin{aligned} f(x) &= f(0) + \frac{f'(0)}{1!} \cdot x + \frac{f''(0)}{2!} \cdot x^2 + ... \\ &\approx 1 + nx \\ &\Rightarrow \{n = -1\} \Rightarrow f(-\alpha) = 1 + \alpha \end{aligned}$$

Hence, by approximating the factor $(1-\alpha)^{-1}$ with $(1+\alpha)$, where $\alpha = (1-\eta)$, P_t^{wall} can be expressed as

$$P_t^{wall} = \begin{cases} (2-\eta) \cdot P_t^{bat} & \text{if } P_t^{bat} \geq 0 \\ \eta \cdot P_t^{bat} & \text{if } P_t^{bat} < 0 \end{cases},$$

which can be written as

$$P_t^{wall} = P_t^{bat} + (1-\eta) \cdot |P_t^{bat}|.$$

4.4 Bucket Model

Changing focus to the BM, the control variable is now the battery power P_t^{bat}. Since the BM was included to simplify calculations and speed up runtime for V2G application in Chapter 5, the problem formulation was set up with the next step in mind. Hence, the additional index i, which corresponds to EV i, and index h, corresponding to household h, were added. However, in this V2H stage, only one EV and one household were considered. The linear program was set up as

$$\min \quad \Pi^{net} + \lambda^{deg,BM} \tag{4.19}$$

$$\text{s.t.} \quad \Pi^{net} = \sum_t \left[\lambda_t^{da} \cdot (\sum_h E_{t,h} + \sum_i P_{t,i}^{wall} \cdot \Delta t) \right] \tag{4.20}$$

$$z_{t+1,i} = \frac{P_{t,i}^{bat}}{b^{cap,kWh}} \Delta t + z_{t,i} \qquad \forall \quad t,i \tag{4.21}$$

$$P^{min} \leq P_{t,i}^{wall} \leq P^{max} \qquad \forall \quad t,i \tag{4.22}$$

$$z^{min} \leq z_{t,i} \leq z^{max} \qquad \forall \quad t,i \tag{4.23}$$

$$z_{t^{start},i} = z_i^{init} \qquad \forall \quad t,i \tag{4.24}$$

$$z_{t^{end}+1,i} \geq z^{end} \qquad \forall \quad t,i \tag{4.25}$$

$$\sum_i P_{t,i}^{wall} \cdot \Delta t \geq -\sum_h E_{t,h} \qquad \forall \quad t \tag{4.26}$$

$$\lambda^{deg,BM} = \sum_i C_i^{lost,BM} \cdot b^{cost} \tag{4.27}$$

$$C_i^{lost,BM} = d_i^{cal} + d_i^{cyc} \qquad \forall \quad i \tag{4.28}$$

$$P_{t,i}^{wall} = P_{t,i}^{bat} + (1-\eta) \cdot |P_{t,i}^{bat}| \qquad \forall \quad t,i \tag{4.29}$$

The objective function remains the same as in (4.5), while constraint (4.20) now includes a summation of the energy consumption of all households and a summation of the wallbox energy exchange for all EVs. In (4.21), the battery capacity has changed to the battery pack energy capacity $b^{cap,kWh}$ and the new index i is included. Constraints (4.22)-(4.25) are identical to (4.8)-(4.11) except for the addition of the index i. Constraint (4.26) restricts the energy discharged from all EVs to be at most the sum of all households' energy consumption. (4.27) calculates the cost of battery degradation for all EVs, where (4.28) yields the capacity loss from calendar aging and cycle aging for the ith EV, described earlier in (3.19). (4.29) remains the same as in the ECM but is given last in this list of constraints to facilitate reuse of constraints in Chapter 5.

4.5 Simulation Over Longer Time Periods

To simulate longer time periods, several optimization problems were solved iteratively. The optimal solution for each subproblem was returned, meaning that the final solution was a combination of local optimums. Two pieces of pseudocode of

the simulation over a time horizon of one year are presented in Algorithm 1 and Algorithm 2 for the ECM and BM, respectively.

Algorithm 1 ECM variant

Initialize parameters according to Table 4.2
$T^{acc} \leftarrow$ Battery age b^{age}, from Table 4.3
$Q^{acc} \leftarrow$ Accumulated throughput, calculated using Table 4.3 and (4.3)
$\Delta SoC \leftarrow$ SoC decrease due to driving, calculated using Table 4.3 and (4.4)
$z^{init} \leftarrow SoC^{ref} - \Delta SoC$
$z^{end} \leftarrow SoC^{ref}$
for $day \leftarrow 1, 364$ **do**
    $Set\ of\ hours \leftarrow \{arrival_{day}, departure_{day+1}\}$
    for each $t \in Set\ of\ hours$ **do**
        $\lambda_t^{da} \leftarrow$ Day-ahead electricity cost for hour t
        $E_t \leftarrow$ Household energy consumption for hour t
    end for
    $\{Optimal\ Variables\} \leftarrow$ Run ECM optimization (4.5) - (4.17)
    $Q^{acc} \leftarrow Q^{acc} + \sum_t |I_t| \cdot \Delta t + \Delta SoC \cdot b^{cap,Ah}$
    $T^{acc} \leftarrow T^{acc} + 1$
    $\Delta \mathrm{DoD}_{day} \leftarrow \Delta \mathrm{DoD}$
end for
$\widehat{\Delta \mathrm{DoD}} \leftarrow \frac{\sum_{i=1}^{364} \Delta \mathrm{DoD}_i}{364}$

Algorithm 2 BM variant

Initialize parameters according to Table 4.2
$T^{acc} \leftarrow$ Battery age b^{age}, from Table 4.3
$Q^{acc} \leftarrow$ Accumulated throughput, calculated using Table 4.3 and (4.3)
$\Delta SoC \leftarrow$ SoC decrease due to driving, calculated using Table 4.3 and (4.4)
$z^{init} \leftarrow SoC^{ref} - \Delta SoC$
$z^{end} \leftarrow SoC^{ref}$
for $day \leftarrow 1, 364$ **do**
    $Set\ of\ hours \leftarrow \{arrival_{day}, departure_{day+1}\}$
    for each $t \in Set\ of\ hours$ **do**
        $\lambda_t^{da} \leftarrow$ Day-ahead electricity cost for hour t
        $E_t \leftarrow$ Household energy consumption for hour t
    end for
    $\{Optimal\ Variables\} \leftarrow$ Run BM optimization (4.19) - (4.28)
    $Q^{acc} \leftarrow Q^{acc} + \frac{\sum_t |P_t^{bat}| \cdot \Delta t}{b^{cap,kWh}} \cdot b^{cap,Ah} + \Delta SoC \cdot b^{cap,Ah}$
    $T^{acc} \leftarrow T^{acc} + 1$
end for

For the BM, the cycle depth ΔDoD had to be assumed from a comparable simulation of the ECM to make the cycle aging linear in the variables. Hence, the ECM was simulated using the User 5 scenario as it represented the average driving behavior

among the scenarios in Table 4.3. From this simulation, the average ΔDoD was extracted and used as the assumed value for the cycle depth in the BM.

4.6 Household Energy Consumption Forecasting

Since the household energy consumption is unknown beforehand when running the optimization in a real-world solution, a forecasting method was included in the thesis. Hourly electricity consumption data was gathered from a household in Gothenburg between the years 2015 and 2021. Data between 2015-2020 was used to train and validate a long short-term memory (LSTM) network to give a forecast on an hourly granularity for the household's energy consumption for the next day. The structure of the LSTM network was inspired by one Jason Brownlee developed for energy consumption prediction in [43], which uses an encoder-decoder model for the network. Table 4.4 shows the layers and the corresponding parameters of the network. Apart from the actual energy consumption from the past 24 hours, the day of the week and month were used as input to the network to capture seasonal effects. The output was the forecast energy consumption for each hour during the following 24 hours.

Table 4.4: Structure of LSTM network in order from input to output.

Layer	No. units	Activation function
LSTM layer	200	ReLU
LSTM layer	200	ReLU
Fully connected layer	100	ReLU
Output neuron	1	-

The LSTM predictions were benchmarked against the naïve method of taking the energy consumption from the last day as a prediction for the next day. A comparison between the root-mean-square error (RMSE) for the LSTM and the baseline is given in Table 4.5.

Table 4.5: Comparison of RMSEs between the LSTM and baseline.

Method	RMSE
LSTM	0.709
Baseline	0.816

Since the LSTM predictions showed a lower RMSE than predictions from the baseline model, the LSTM was chosen to produce the predictions. Nevertheless, predicting energy consumption for a single household is a complex task due to the high variance in both consumption and during which hours increased or decreased consumption happens. Rather than spending a considerable amount of time trying to improve the predictions given that energy consumption forecasting was not part of the thesis aim, we focused more on the formulation and solution of the optimization problems in the thesis.

4.7 Benchmark Models

Two benchmark models were developed to quantify the potential of utilizing V2H. Both models only allowed unidirectional charging, meaning that no discharging was allowed. The first model, uncontrolled charging (UC), was set up such that the EV was charged to the reference SoC as quickly as possible when plugged in after arrival at the household. The second model, smart charging (SC), minimized the EV charging cost by scheduling the charging required to reach the reference SoC to the cheapest available hours within the optimization horizon. An example of smart charging is visualized in Figure 4.2, in which the EV is charged during the two cheapest hours within the time frame, with maximum power during the cheapest hour.

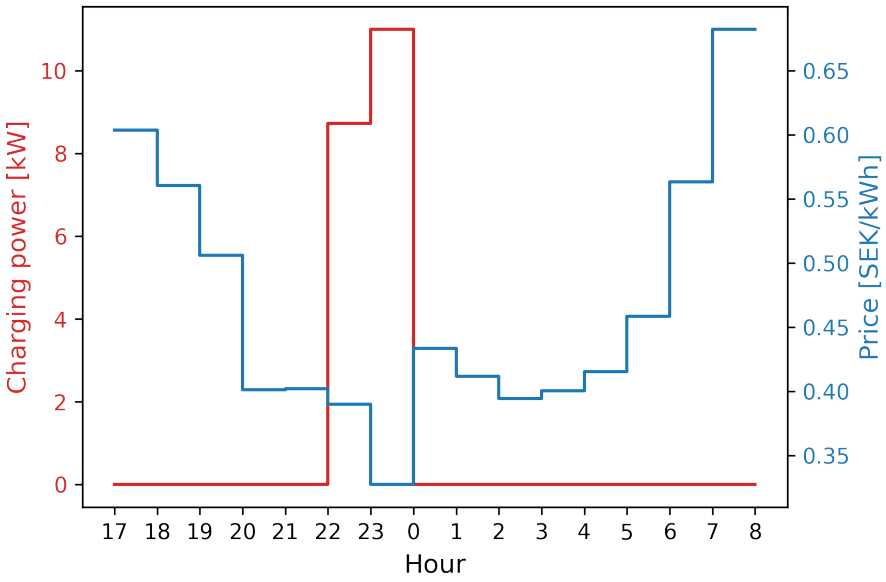

Figure 4.2: Example of smart charging within an optimization horizon.

The results from these two models will be presented as benchmarks in comparison with the V2H results.

4.8 Results

The V2H results are based on the different usage scenarios given earlier in Table 4.3. As a reminder, the driving distance per year and the battery age for the different user scenarios are repeated once again in Table 4.6.

Table 4.6: Recapitulation of different user scenarios.

	d^{dist} [km]	b^{age} [days]
User 1	3,650	30
User 2	3,650	365
User 3	3,650	1,095
User 4	11,120	30
User 5	11,120	365
User 6	11,120	1,095
User 7	36,500	30
User 8	36,500	365
User 9	36,500	1,095

The results will be presented using electricity prices and the predicted household energy consumption data for 2021. The predicted household energy consumption excluding EV charging during the 5,772 hours within the optimization horizons of 2021 was calculated to cost 6,397 SEK, using the day-ahead prices for price region SE3 obtained from [44]. For every user, the three different models UC, SC, and V2H are compared. A corresponding table using the actual household energy consumption data can be found in Appendix A.

4.8.1 Equivalent Circuit Model

The results for uncontrolled charging, smart charging, and V2H using the ECM and predicted energy consumption are presented for the different users in Table 4.7.

Table 4.7: Comparisons of different user scenarios in the ECM, predicted household energy consumption.

		Energy cost [SEK]	Cyc. cost [SEK]	Cal. cost [SEK]	Total [SEK]	Savings
User 1	UC	7,041	168	1,383	8,592	-
	SC	6,670	186	1,364	8,220	4.3%
	V2H	5,401	697	1,349	7,447	13.3%
User 2	UC	7,041	92	1,039	8,172	-
	SC	6,670	102	1,025	7,797	4.6%
	V2H	5,209	629	1,010	6,848	16.2%
User 3	UC	7,041	60	837	7,938	-
	SC	6,670	66	825	7,561	4.7%
	V2H	5,063	570	810	6,443	18.8%
User 4	UC	8,358	307	1,382	10,047	-
	SC	7,230	388	1,330	8,948	10.9%
	V2H	5,836	852	1,307	7,995	20.4%
User 5	UC	8,358	169	1,038	9,565	-
	SC	7,230	213	999	8,442	11.7%
	V2H	5,652	687	979	7,318	23.5%
User 6	UC	8,358	109	836	9,303	-
	SC	7,230	137	804	8,171	12.2%
	V2H	5,488	604	785	6,877	26.1%
User 7	UC	12,884	802	1,369	15,055	-
	SC	9,167	1,077	1,227	11,471	23.8%
	V2H	7,874	1,335	1,189	10,398	30.9%
User 8	UC	12,884	440	1,029	14,353	-
	SC	9,167	590	922	10,679	25.6%
	V2H	7,649	964	887	9,500	33.8%
User 9	UC	12,884	284	828	13,996	-
	SC	9,167	381	742	10,290	26.5%
	V2H	7,502	762	708	8,972	35.9%

The column *Energy cost [SEK]* shows the household energy cost using the predicted household energy consumption, including EV charging. *Cyc. cost [SEK]* indicates the battery degradation cost due to cycle aging, while *Cal. cost [SEK]* specifies the battery degradation cost caused by calendar aging. The column *Total [SEK]* summarizes the total cost of household electricity, EV charging, cycle aging, and

calendar aging during the optimization hours. *Savings* indicates the percentage of savings compared with the case of uncontrolled charging for the *Total [SEK]* column. The table is also visualized as a bar plot in Figure 4.3.

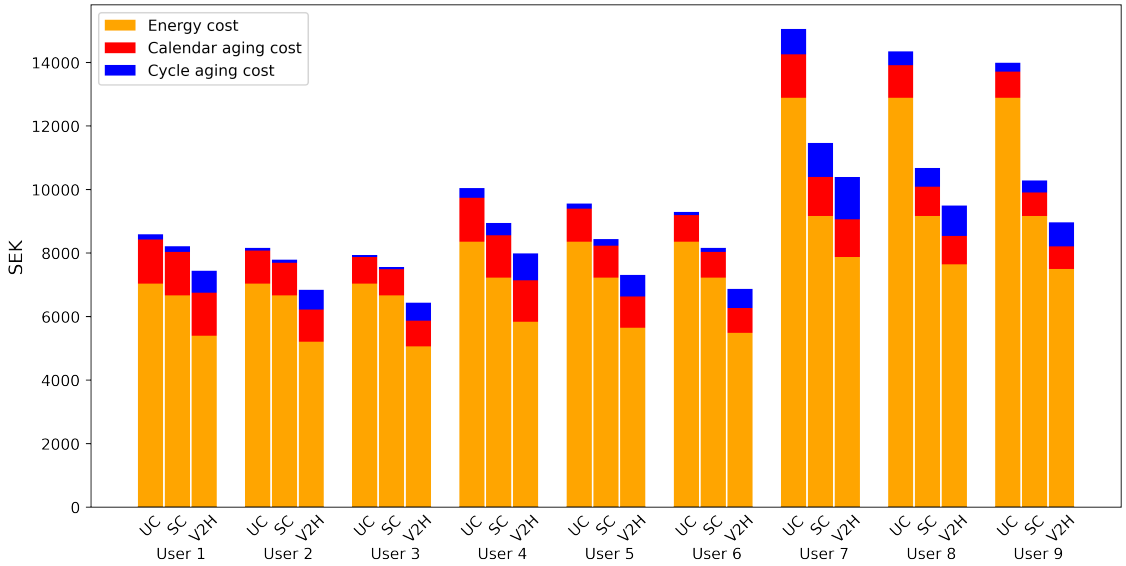

Figure 4.3: Graphical visualization of costs related to each user scenario.

The charging power as seen from the wallbox for User 1, User 5, and User 9 utilizing V2H is visualized in Figure 4.4. The day of the year is on the horizontal axis, and the hour of the day is on the vertical axis. The colors indicate the charging power as seen from the wallbox. Figures for the other users can be found in Appendix A.

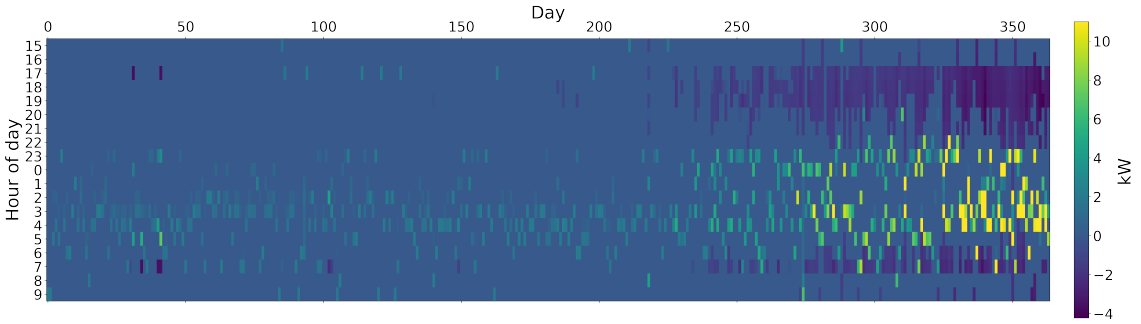

(a) User 1

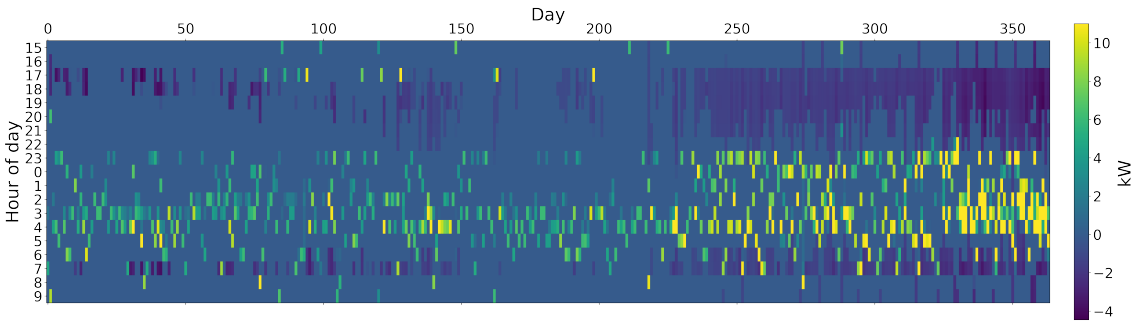

(b) User 5

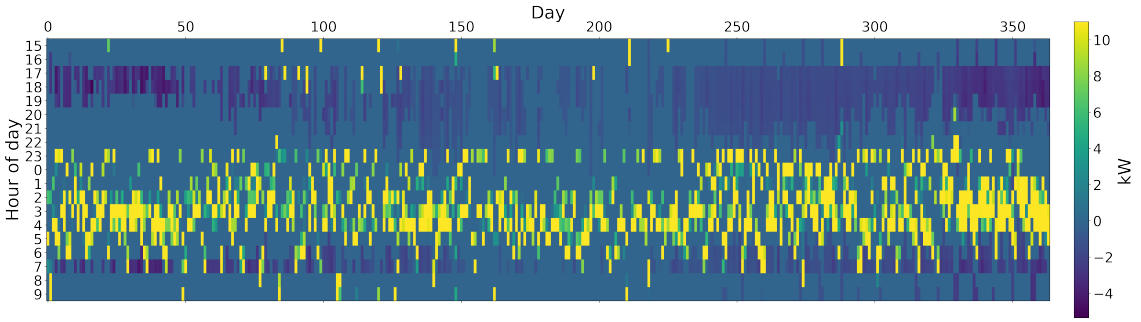

(c) User 9

Figure 4.4: V2H charging power as seen from the wallbox.

The corresponding development of battery capacity loss due to calendar aging and cycle aging for User 1, User 5, and User 9 within the period of optimization is shown in Figure 4.5. To facilitate comparisons, the same axis scales were used. Additional plots for the other users can be found in Appendix A.

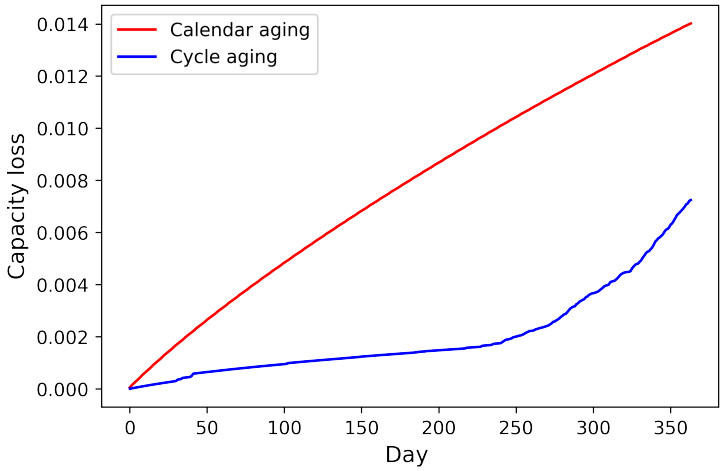

(a) User 1

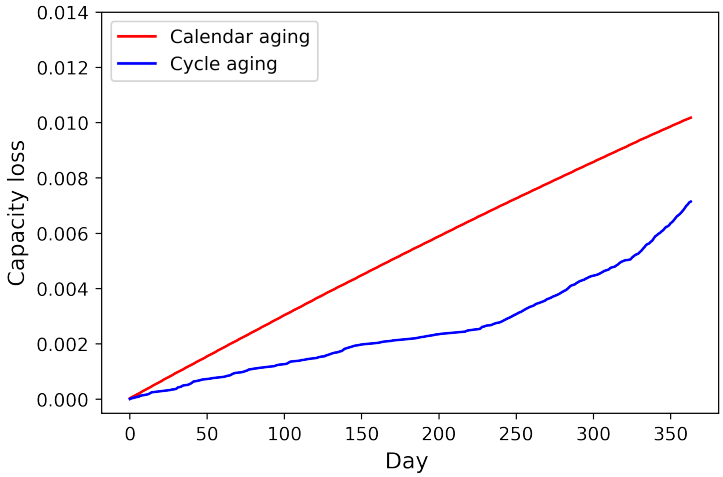

(b) User 5

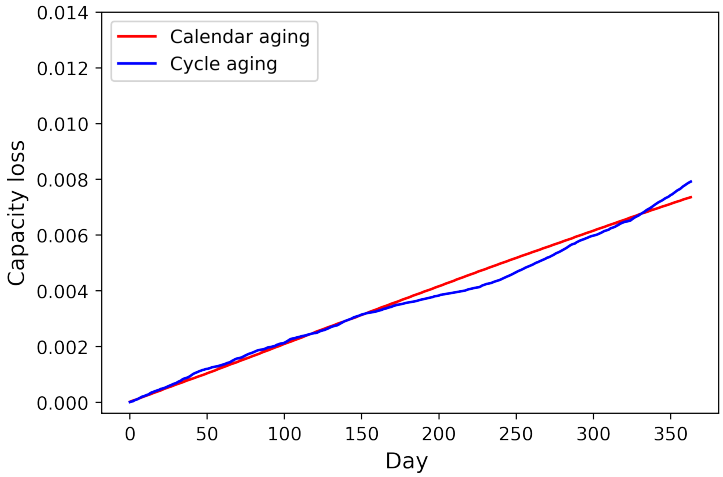

(c) User 9

Figure 4.5: Development of normalized capacity loss due to battery aging, for V2H.

4.8.2 Comparison Between ECM and BM

Table 4.8 was included to compare the accuracy of the BM versus the ECM and motivate the use of the BM in Chapter 5. The comparison was made for the V2H scenario, using the predicted household energy consumption.

Table 4.8: Comparison between the ECM and BM for the V2H case using predicted household energy consumption.

		Energy cost [SEK]	Cyc. cost [SEK]	Cal. cost [SEK]	Total [SEK]
User 1	ECM	5,401	697	1,349	7,447
	BM	5,343	716	1,346	7,405
User 2	ECM	5,209	629	1,010	6,848
	BM	5,191	625	1,007	6,823
User 3	ECM	5,063	570	810	6,443
	BM	5,028	577	808	6,413
User 4	ECM	5,836	852	1,307	7,995
	BM	5,809	910	1,306	8,025
User 5	ECM	5,652	687	979	7,318
	BM	5,570	707	975	7,252
User 6	ECM	5,488	604	785	6,877
	BM	5,403	602	779	6,784
User 7	ECM	7,874	1,335	1,189	10,398
	BM	7,639	1,277	1,195	10,111
User 8	ECM	7,649	964	887	9,500
	BM	7,420	825	889	9,134
User 9	ECM	7,502	762	708	8,972
	BM	7,379	577	714	8,670

4.9 Discussion

Table 4.7 and Figure 4.3 display the potential of V2H compared with uncontrolled charging and smart charging. One can see that the cycle aging cost increases with V2H utilization, while the calendar aging cost decreases. Combining both degradation factors, the overall cost of battery degradation increases with V2H. However, the lowered cost of household energy overcompensates for this effect. Though, we still want to stress the importance of including the increased cost of battery degradation when considering bidirectional charging strategies. By analyzing the numbers in Table 4.7, it can be observed that the increased cost of battery degradation comprises up to 30.2% of the total energy cost savings made by utilizing V2H compared with uncontrolled charging.

Looking specifically at the different user scenarios, long-distance drivers (User 7-9) have a higher potential to make a saving from smart charging and V2H compared with uncontrolled charging. The explanation is that electricity prices often are high when the EV returns to the household, and this cluster of drivers needs to charge their EVs with more energy due to their driving pattern. When comparing smart charging and V2H, short-distance drivers (User 1-3) and average-distance drivers (User 4-6) generally save more percentage points compared with the long-distance drivers. The intuition behind this is that long-distance drivers have a higher charging demand, leading to less flexibility in utilizing V2H.

Regarding the calendar aging, one can infer from Table 4.7 that both smart charging and V2H lowers the calendar aging compared with uncontrolled charging. Since the formula for calendar aging uses the average voltage, which in turn can be related to the average SoC, uncontrolled charging leads to a higher average SoC within each optimization horizon compared with smart charging and V2H, resulting in a higher cost of calendar aging. Since V2H also allows for discharging, the average SoC can be reduced even further when compared with smart charging, leading to a lower calendar aging effect for V2H.

Looking at Figure 4.4, depicting the charging power as seen from the wallbox for User 1, User 5, and User 9 utilizing V2H, one can see that the charging behaviors differ drastically between the users. User 1, the short-distance driver with a 30-day-old battery, utilizes V2H rarely during the first half of the year due to the high marginal cost of cycle aging. Throughout the year, battery cell throughput is accumulated due to driving and charging. This results in a lower cycle aging marginal cost later in the year, with more V2H utilization. Moreover, this behavior can also be tracked down to the difference between the highest and lowest electricity prices within each single optimization horizon. As seen in Figure 4.6, this price difference was smaller at the beginning of 2021, reducing the potential to make a saving on V2H when also considering the cost of battery degradation, while the price difference was larger at the end of 2021.

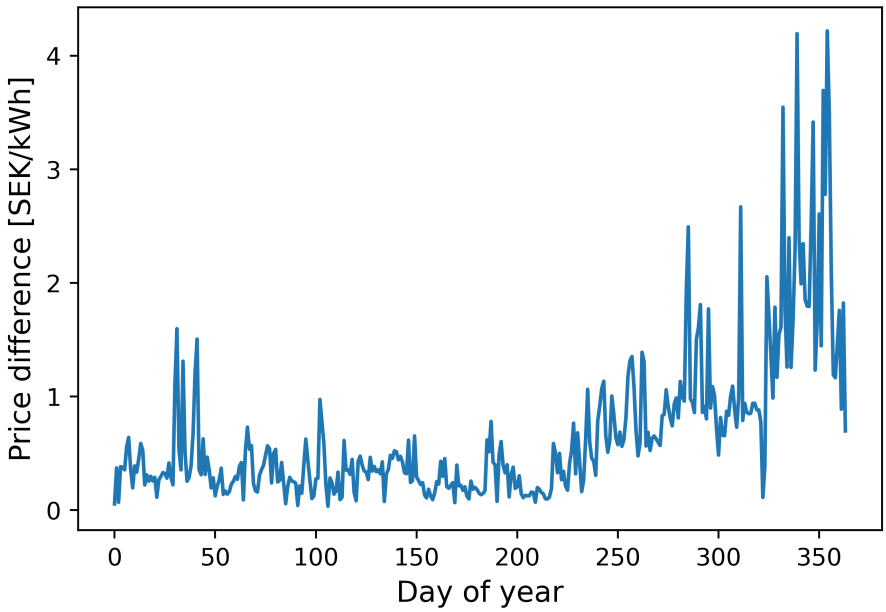

Figure 4.6: Difference between the highest and lowest hourly electricity price within each optimization horizon of 2021.

User 5, the average-distance driver with a 1-year-old battery, utilizes V2H more compared with User 1. The battery has been cycled more due to the increased driving demand and the older battery, leading to a lower marginal cost for cycle aging. The long-distance driver with a 3-year-old battery, User 9, utilizes V2H to a high degree even at the beginning of the year. Since the battery has been cycled substantially during the first three years due to the driving behavior, the marginal cost for cycle aging is low. This makes V2H profitable even when the price difference between the highest and lowest electricity prices is small.

Analyzing the development of the battery capacity loss in Figure 4.5, the capacity loss due to calendar aging differs drastically between the three users. This is expected, since an older battery has a moderate slope of the calendar aging tangent compared with a newer battery, as visualized earlier in Figure 3.4. As a consequence, one can see more curvature in the development of the calendar aging effect for User 1, while almost a straight line is seen for User 9. Shifting the focus to the capacity loss caused by cycle aging, it ends on almost the same level for all three users, around 0.8%. The explanation behind this is that User 1 has a high marginal cost for cycle aging, but at the same time cycles the battery to a low degree, while User 5 and User 9 have lower marginal costs for cycle aging, but cycles the battery substantially more. Similarly, as for the calendar aging effect, there is a curvature in the cycle aging development for User 1, while one can observe less curvature for User 5, and a closer to linear behavior for User 9. Once again, this is explained by a decreasing slope of the cycle aging tangent, in combination with the driving pattern of User 9 which requires charging of almost 24% SoC per day.

However, some doubts exist regarding the method for implementing the degradation model, specifically for the cycle aging. The authors of the paper describing the degradation model let batteries cycle with different amplitudes around different voltages, and the impact of the specific behavior was measured once every three weeks [4]. In that way, the depth of discharge ΔDoD would remain constant throughout the lifetime of the battery. When this degradation model was implemented in the V2H optimization problem, the degradation formula was reformulated to capture the effect of a certain behavior during one particular optimization horizon. For the cycle aging, this would for instance imply that the aging would not be directly dependent on the historical ΔDoD, although some information regarding the historical usage is obtained through the accumulated throughput. As this reformulation has not been verified through experiments, it is uncertain how close the modeled degradation is to the true degradation. Moreover, it is not clear how to correctly model the ΔDoD. The method used in this work was suggested by [33] and it calculates the average deviation from the average SoC during the optimization horizon. This method accurately captures the effect when the SoC is fairly symmetric around its mean during the optimization horizon which, by inspection, seems to be the case for V2H. However, for cases when this is not true, the above-mentioned method yields questionable results. Imagine for instance the case of uncontrolled charging. Directly after being plugged in, the EV will be charged with full power until it reaches the desired SoC. Following this, the SoC will remain constant until the end of the horizon. By assuming that the desired SoC is reached in a small fraction of the total length of the horizon, the average SoC in the horizon will be close to the desired SoC, and the ΔDoD encoded as the average distance from the mean SoC, will be relatively low. However, if the charging had happened in the middle of the horizon, the ΔDoD would be higher as the average distance from the mean SoC would be higher. Hence, even if the batteries were cycled with the same throughput, the calculated ΔDoD, and consequently the cycle aging, would be different. This phenomenon is likely the reason why the cycle aging cost differs between uncontrolled charging and smart charging in Table 4.7, where it is underestimated for uncontrolled charging.

The comparison between the ECM and the BM shows that the two models coincide to an acceptable level, considering that the BM uses several assumptions to make the optimization problem linear. The calendar aging cost follows well for all users, while the cycle aging cost varies more. This variation is expected since the $\widehat{\Delta\text{DoD}}$ was approximated as a fixed value using the average ΔDoD from the ECM User 5 simulation, leading to a fixed value of β in the cycle aging function for the BM. One noticeable detail is that the energy cost is lower for the BM for every user scenario. This was tracked down to be due to the solver in the nonlinear ECM not finding the exact optimal solution every time, while the solver for the linear BM found the actual optimum.

Lastly, since the optimization setting the optimal power exchange schedule is run before the start of the time horizon, real-world implementation of the V2H optimization requires an accurate household energy consumption forecast. However, the energy consumption in a single household is fairly unpredictable, with sudden consumption peaks and unforeseen low consumption. To establish a more accurate prediction model, the user should be able to input planned increases and decreases in energy consumption due to, for instance, travels or vacation. One could also imagine that the V2H scheduler would communicate with other smart appliances in the household, e.g., a heating pump, to obtain a better forecast.

5
Vehicle-to-Grid

With the results from the V2H scenarios obtained, the next thesis aim was to extend the V2H problem formulation into a combined V2H and V2G problem formulation, which simply will be referred to as V2G throughout the chapter. In the V2G optimization problem, a fleet of EVs with their corresponding households have been examined to, in addition to utilizing V2H, offer capacity for frequency regulation to the TSO. Figure 5.1 displays how a fleet of EVs connected to their households jointly can offer a V2G service.

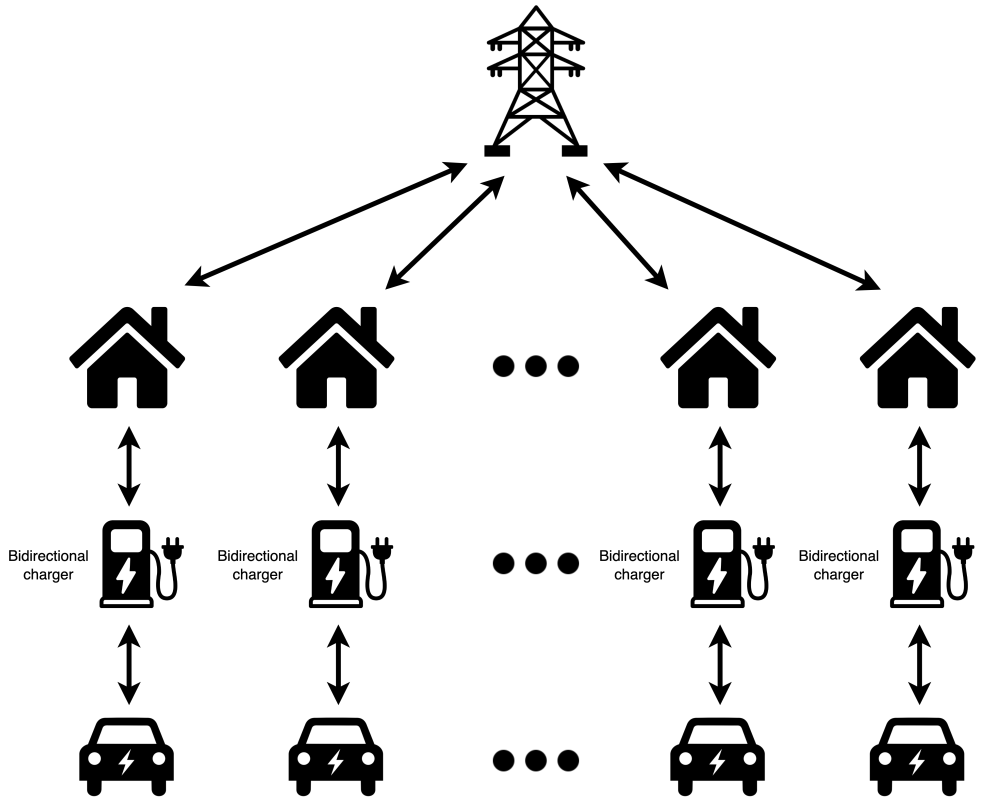

Figure 5.1: Visualization of power flow directions for a fleet of EVs in a V2G solution.

Two different deterministic linear optimization problems were set up to extend V2H with the possibility to also offer frequency regulation, for the products FCR-N and FCR-D up in the Swedish market. As with the optimization problems related to V2H, the V2G optimization problems were modeled using Pyomo [36], [37]. As the

V2G problems were linear, there was no need to use a nonlinear solver. Instead, a more efficient linear solver could be used. The solver Gurobi was chosen for this task [45]. Unless other stated, the relevant parameter values from Table 4.2 were reused in this chapter. Before introducing the optimization problems further, the assumptions made will be described.

5.1 Assumptions

The following subsections will describe the assumptions made in the V2G chapter.

5.1.1 Choice of Days

Due to increased computational complexity when involving a fleet of EVs, the optimization problems were set up to run during four different dates instead of a whole year. The dates were chosen arbitrarily but with the intention to spread the days between the seasons of the year. The dates are shown in Table 5.1.

Table 5.1: Dates and times for optimization in the V2G case.

	Date	Arrival time	Departure time
Day 1	11th-12th Jul 2021	17:00	8:00
Day 2	11th-12th Oct 2021	17:00	8:00
Day 3	11th-12th Jan 2022	17:00	8:00
Day 4	11th-12th Apr 2022	17:00	8:00

5.1.2 Individual EV Attributes

Assumptions were also made regarding the average driving distance per day, the battery age, and the arrival SoC for each EV. These three were sampled from different truncated Gaussian distributions, as summarized in Table 5.2.

Table 5.2: Truncated Gaussian distribution parameters used for sampling.

	Mean	St. dev.	Min	Max
Avg. driving distance	30 km	20 km	5 km	100 km
Battery age	365 days	365 days	30 days	1,095 days
Arrival SoC	0.45	0.10	0.35	0.55

The distributions of average driving distance per day and battery age were necessary to calculate the degradation factor for each EV. The means were set according to the values of the average user in Section 4.2, User 5, while the maximum values were set according to the extreme user, User 9. The lower limit for average driving distance per day was set to 5 km, and for battery age, it was set to 30 days. The standard deviations were set to 20 km and 365 days, respectively. As previously discussed, the BM also needs an assumption on the $\widehat{\Delta \text{DoD}}$ for the problem to remain linear.

This was chosen to be the average ΔDoD obtained from the User 5 scenario when utilizing V2H with the ECM. As a consequence, it was of interest to sample the arrival SoC levels such that the values were close to the assumed arrival SoC of User 5. This motivated the choice of mean, standard deviation, and limits for the truncated Gaussian distribution. The end SoC, z^{end}, was set to be at least 0.70, or 70%, for all EVs.

5.1.3 Prices and Activation

For each day, day-ahead prices [44] and regulation prices [46] were acquired from Nord Pool. The remunerations for offering regulation bids were collected from Svenska Kraftnät's website Mimer [47].

Additionally, the dispatch to contract ratio R_t^{D2C} used in the FCR-N formulation was assumed to be known beforehand for every hour within the optimization horizon. The dispatch to contract ratio quantifies the proportion of the offered bid that has to be activated. It was calculated using the historical frequency of the Nordic Synchronous System according to

$$R_t^{D2C} = \begin{cases} \max\left(\frac{f_t - 50.00}{50.00 - 49.90}, -1\right) & \text{if } f_t < 50.0 \\ \min\left(\frac{f_t - 50.00}{50.00 - 49.90}, 1\right) & \text{if } f_t \geq 50.0 \end{cases},$$

where f_t is the frequency with the maximum deviation from 50.00 Hz within hour t. The frequency data collected from Fingrid [48] had a resolution of 3 minutes. By selecting the frequency with the maximum deviation from 50.00 Hz within each hour as the hourly frequency, a "worst-case" activation was achieved. The resulting activation profiles for the different days are shown in Figure 5.2. Note that a negative activation implies that the frequency was lower than 50.00 Hz.

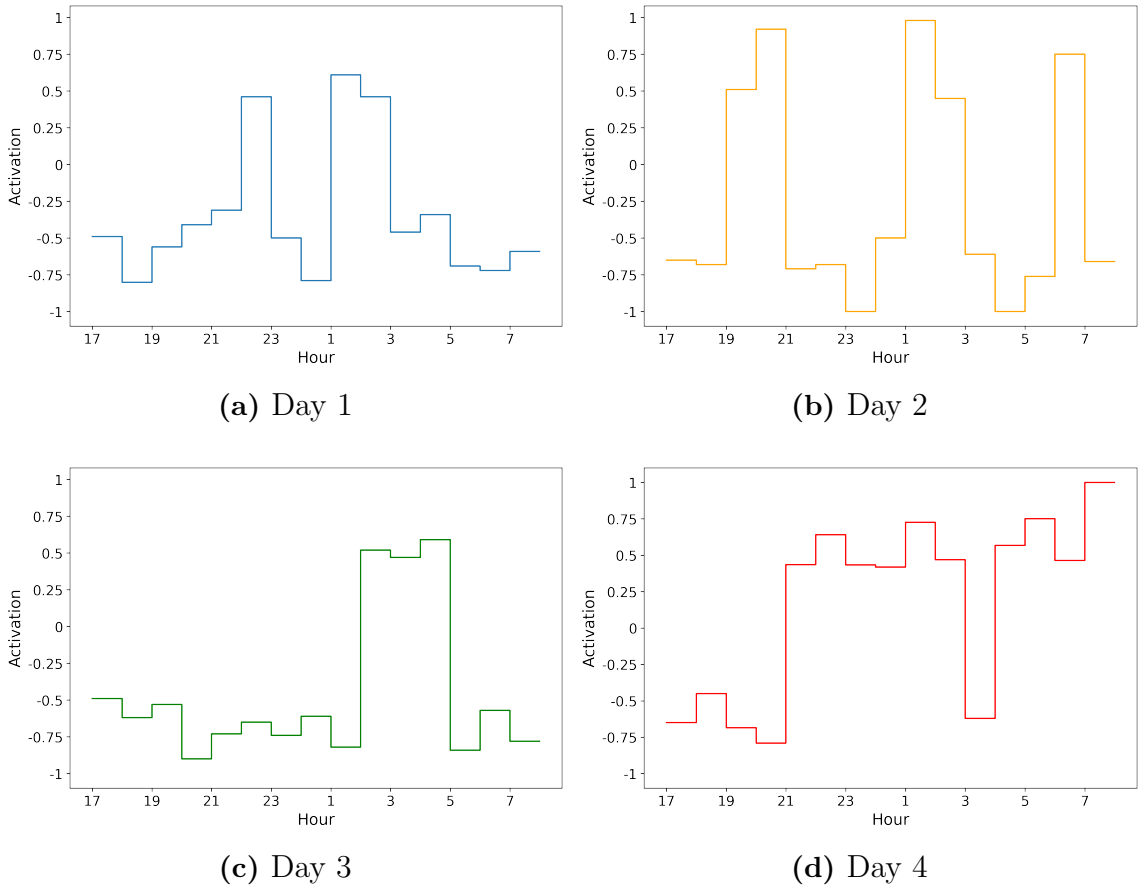

(a) Day 1 **(b)** Day 2

(c) Day 3 **(d)** Day 4

Figure 5.2: Assumed activation of FCR-N for Days 1-4.

The assumption made for FCR-D up activation was different. As discussed in Section 2.2.1, it is rare that the frequency of the grid deviates to such magnitude that FCR-D up resources must be activated to a high degree. For instance, there was only one moment during 2020 when the deviation of the frequency of the Nordic synchronous system required 100% activation of FCR-D up resources. The deviations were also restored quickly, meaning that FCR-D up resources are not active for long periods. As a reference, between 0-25% of FCR-D up resources were activated 26,456 times during 2020 according to Table 2.1. As the average duration of the deviations was 9.6 s, this resulted in approximately 70.5 h of activation in the specified region in total throughout the year. This corresponds to 0.19 h per day when distributing the activation evenly throughout the year. The resulting SoC change during one day of a worst-case activation within the interval 0-25% would hence correspond to

$$\frac{0.19 \text{ h} \cdot 11 \text{ kW}}{78 \text{ kWh}} \cdot 0.25 \approx 0.7\%.$$

This calculation was used to motivate the neglect of the activation of the resources in the optimization problem for FCR-D up.

5.1.4 Household Energy Consumption

While hourly household energy consumption from only one household was used for V2H in Chapter 4, it was desired to use data from several households for the V2G simulations. Hourly consumption data from three households in Sweden were collected and used deterministically, and no predictions were made. The households' energy consumption during the selected days is shown in Figure 5.3. Day 1 was in the middle of the summer, explaining the significantly lower energy consumption compared with the other days.

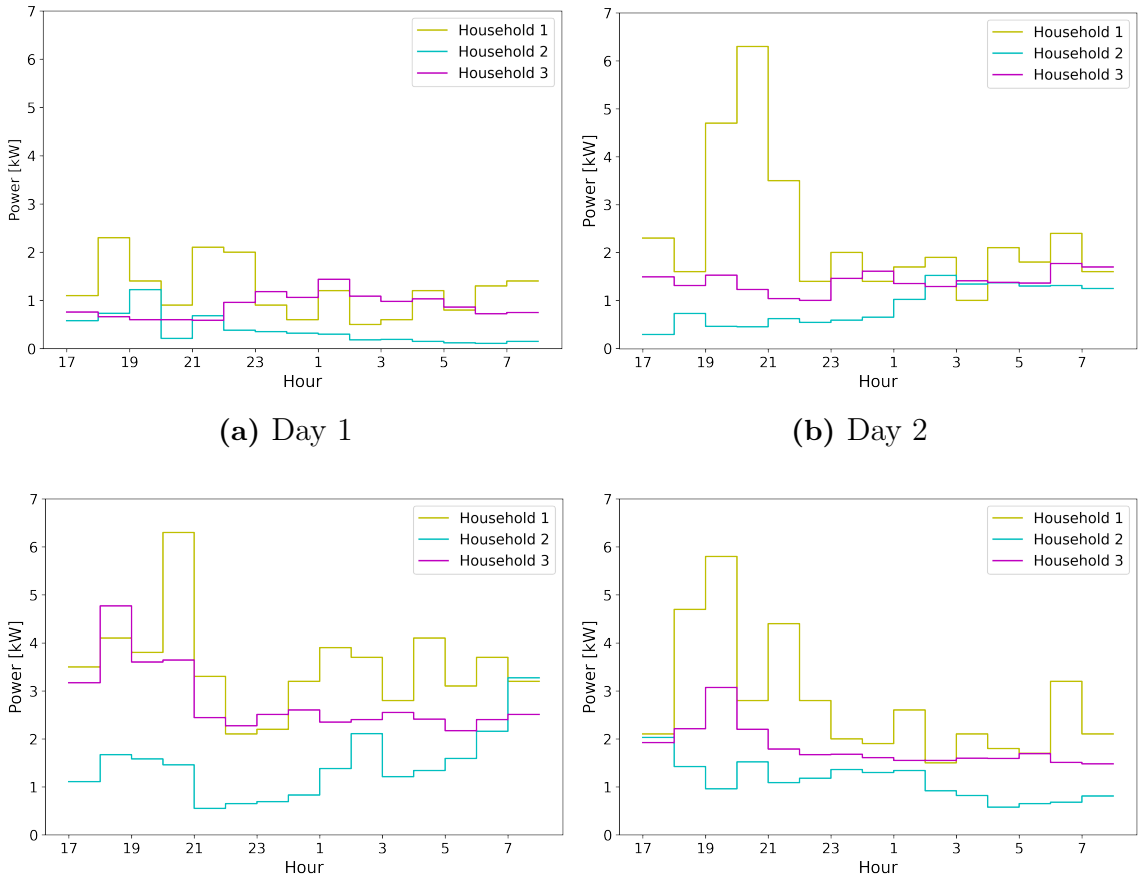

(a) Day 1 **(b)** Day 2

(c) Day 3 **(d)** Day 4

Figure 5.3: Energy consumption for households 1-3 during the selected days.

To accommodate larger fleet sizes than three, the respective households' energy consumption were duplicated several times to synthetically create a larger dataset with an equal number of samples from each household.

5.2 FCR-N

For offering frequency regulation through FCR-N, the bid has to be symmetrical in both up and down directions. To upregulate the frequency, the EVs can either stop charging or start discharging. To downregulate the frequency, the EVs can increase charging. Inspired by [8], the optimization problem was set up according to

$$\min \quad \Pi^{net} - \Pi^{bid} + \Pi^{reg} + \lambda^{deg,BM} \tag{5.1}$$

$$\text{s.t.} \quad \text{Constraints (4.20)} - \text{(4.28)}$$

$$\Pi^{bid} = \sum_t \lambda_t^{b,FCR-N} \cdot R_t^b \tag{5.2}$$

$$\Pi^{reg} = \sum_t \lambda_t^r \cdot R_t^{D2C} \cdot R_t^b \tag{5.3}$$

$$R_t^b \leq \sum_i \left[P_{t,i}^{wall} + |P_i^{min}| \right] \qquad \forall \quad t \tag{5.4}$$

$$R_t^b \leq \sum_i \left[P_i^{max} - P_{t,i}^{wall} \right] \qquad \forall \quad t \tag{5.5}$$

$$P_{t,i}^{wall} + \frac{R_t^{D2C} \cdot R_t^b}{|\mathcal{I}|} = P_{t,i}^{bat} + (1-\eta) \cdot |P_{t,i}^{bat}| \qquad \forall \quad t, i \tag{5.6}$$

The objective value (5.1) is the sum of the net electricity costs for all households as in (4.20), the reimbursement from offered regulation bids (5.2), the cost/income from bought/sold energy from activation (5.3), and the cost of battery degradation. (5.4) defines the maximum possible upregulation bid for hour t as the sum of the charging power during hour t, and the absolute value of the maximum possible discharging power during hour t. Similarly, (5.5) defines the maximum possible downregulation bid for hour t as the difference between the charging power during hour t and the maximum possible charging during hour t. Constraint (5.6) is a modification of (4.29) to reflect the activation of the offered bid in the battery power of each EV, and hence let the SoC levels of the EVs be affected by the activation. The activation is set to be equally distributed over all EVs, where $|\mathcal{I}|$ is the number of EVs in the fleet. Constraints (4.20) - (4.28) were reused.

5.3 FCR-D up

The optimization problem for offering FCR-D up was set up as

$$\begin{aligned}
\min \quad & \Pi^{net} - \Pi^{bid} + \lambda^{deg,BM} && && (5.7)\\
\text{s.t.} \quad & \text{Constraints } (4.20) - (4.28) && && \\
& \Pi^{bid} = \sum_t \lambda_t^{b,FCR-D} \cdot R_t^b && && (5.8)\\
& R_t^b \leq \sum_i \left[P_{t,i}^{wall} + |P_i^{min}| \right] && \forall \quad t && (5.9)\\
& P_{t,i}^{wall} = P_{t,i}^{bat} + (1-\eta) \cdot |P_{t,i}^{bat}| && \forall \quad t,i && (5.10)
\end{aligned}$$

The FCR-D up objective (5.7) consists of the net household electricity cost, minus the revenue from offering the FCR-D up bids defined in (5.8), plus the cost of battery degradation. The regulation bid only needs one constraint in the FCR-D up case, namely that the EVs can stop charging and start to fully discharge, as explained by (5.9). As opposed to the FCR-N case, the efficiency formula from the BM is repeated in (5.10), as no activation is being considered. Constraints (4.20) - (4.28) were once again reused.

5.4 Results

In this section, results are shown for offering FCR-N and FCR-D up during the four different days stated among the assumptions in Section 5.1.

Table 5.3 contains the results of offering FCR-N and FCR-D up using a fleet size of 1,000 EVs and 1,000 households. These results are compared with SC and V2H-G, where the latter represents performing V2H on the grid level, i.e., the problem formulated in Section 4.4 while including all households. This implies that an EV from one household can supply energy to another household. The reported values are the mean values obtained when sampling the uncertain parameters and running the optimization for each day three times. It was noticed that the variance of the obtained values was low when running the optimization on the different samples. Hence, it was not deemed necessary to increase the number of samples before calculating the mean.

Table 5.3: Comparisons of different days, using a fleet size of 1,000 EVs.

		Direct cost [SEK]	Cyc. cost [SEK]	Cal. cost [SEK]	Total [SEK]	Savings
Day 1	SC	19,202	4,020	3,348	26,571	-
	V2H-G	18,911	4,115	3,334	26,359	0.8%
	FCR-N	-28,301	5,341	3,618	-19,342	172.8%
	FCR-D	-59,027	4,116	3,334	-51,578	294.1%
Day 2	SC	25,588	4,020	3,342	32,950	-
	V2H-G	15,606	6,609	3,208	25,424	22.8%
	FCR-N	-55,721	11,363	2,929	-41,429	225.7%
	FCR-D	-78,792	7,188	3,310	-68,294	307.3%
Day 3	SC	47,504	4,020	3,378	54,902	-
	V2H-G	16,711	11,012	3,035	30,758	44.0%
	FCR-N	-32,693	9,149	2,937	-20,608	137.6%
	FCR-D	-55,228	11,211	3,041	-40,976	174.6%
Day 4	SC	52,679	4,020	3,421	60,120	-
	V2H-G	27,620	8,698	3,139	39,457	34.4%
	FCR-N	-6,116	10,830	2,796	7,510	87.5%
	FCR-D	-24,050	8,590	3,163	-12,297	120.5%

The column *Direct cost [SEK]* includes the entire fleet cost of EV charging, household energy, reimbursement from offering regulation bids for cases FCR-N and FCR-D, and cost/return from activation for case FCR-N. *Cyc. cost [SEK]* and *Cal. cost [SEK]* sum the total cycle aging cost and calendar aging cost for all EVs, respectively. *Total [SEK]* summarizes all costs and returns, while the column *Savings* compares the percentage of savings for the three cases V2H-G, FCR-N, and FCR-D compared with smart charging.

A corresponding table for a smaller fleet size of 500 EVs and 500 households is shown in Table 5.4.

Table 5.4: Comparisons of different days, using a fleet size of 500 EVs.

		Direct cost [SEK]	Cyc. cost [SEK]	Cal. cost [SEK]	Total [SEK]	Savings
Day 1	SC	9,600	2,047	1,677	13,324	-
	V2H-G	9,453	2,095	1,670	13,218	0.8%
	FCR-N	-14,154	2,704	1,812	-9,638	172.3%
	FCR-D	-29,515	2,096	1,670	-25,749	293.3%
Day 2	SC	12,789	2,047	1,674	16,510	-
	V2H-G	7,797	3,343	1,607	12,747	22.8%
	FCR-N	-27,862	5,691	1,467	-20,704	225.4%
	FCR-D	-39,423	3,649	1,660	-34,114	306.6%
Day 3	SC	23,759	2,047	1,692	27,498	-
	V2H-G	8,411	5,486	1,520	15,417	43.9%
	FCR-N	-16,377	4,628	1,471	-10,278	137.4%
	FCR-D	-27,562	5,595	1,523	-20,444	174.4%
Day 4	SC	26,333	2,047	1,713	30,093	-
	V2H-G	13,821	4,362	1,573	19,756	34.4%
	FCR-N	-3,008	5,398	1,404	3,794	87.4%
	FCR-D	-12,017	4,311	1,586	-6,120	120.3%

5.5 Discussion

As a short remark, caution should be taken when comparing results given in Section 5.4. Since the households' energy consumption differ between the days, it is not straightforward to draw conclusions by comparing numbers across different days. Therefore, the focus of this section will be to compare and discuss intraday results.

The results for FCR-N show a great potential to make a saving by offering the frequency regulation service. For three out of four days, the total cost became negative, meaning that the cost turned into a profit since the return from offering bids overcompensated for the cost of household energy consumption, EV charging, activation, and battery degradation. Although the FCR-N results look promising, the problem formulation is made with knowledge about the activation due to frequency deviations. This is an oversimplification, as frequency deviation information is unknown beforehand. Moreover, the frequency of the grid deviates momentarily, meaning that a granularity of 1 hour cannot be used in a real-world solution. The frequency can easily deviate from 49.90 to 50.10 Hz within one hour, or vice versa, implying that the activation assumed for the FCR-N case in this thesis is a very rough estimation. However, the intention of examining FCR-N was to quantify the financial potential of offering FCR-N, rather than providing an implementable solution. Without knowledge about future activation, a conservative solution would be to offer FCR-N using unidirectional charging solely, i.e., stop charging or charge more than planned, as this would not risk depleting the batteries.

Focusing on FCR-D up, this case yields the lowest total cost for all of the four days, with negative total costs implying profits. As mentioned in Section 5.3, the activation of FCR-D up was ignored since it, on average, would affect the SoC levels and charging behavior of the EVs minimally. Offering the rarely activated product FCR-D up shows great numbers in terms of savings, while only adjusting the charging behavior minimally.

Looking specifically at Day 1, 11th-12th of July 2021, it can be seen that V2H-G barely makes a saving compared with smart charging. This was due to the combination of very low variance of the electricity prices within the optimization horizon, which can be seen in Figure 5.4, and low household energy consumption as previously seen in Figure 5.3. The cost of cycle aging was higher than the price difference for every hour, except for the last hour when the electricity price more than doubled. During that specific hour, the EVs were discharged to the households and a small saving compared with smart charging was obtained.

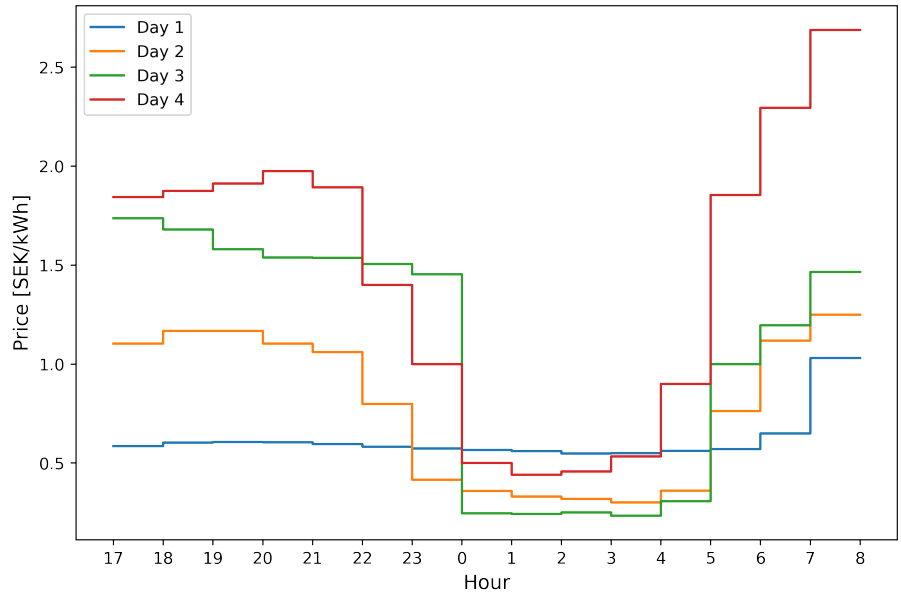

Figure 5.4: Development of hourly electricity prices for Days 1-4.

Comparing the two tables Table 5.3 and Table 5.4, one can identify that the costs scale almost linearly with the number of EVs and households. This is simply a consequence of the small sample of households and their respective energy consumption. Due to the lack of data, as previously mentioned, the households' energy consumption was repeated several times to create larger samples. If we would possess actual household energy consumption data from the desired number of households, the results may not scale linearly between 500 EVs and 1,000 EVs.

For FCR-D up, it can be seen that the cycle aging cost was above the corresponding V2H-G cycle aging cost for three out of four days. Intuitively, this was not expected since no activation was included for FCR-D up. After further investigation, this is explained by the formulation of the possible bid size for FCR-D up. The bid during one hour is a combination of what the EVs can discharge in the specific hour, plus the charging power that can be turned off. Hence, if the remuneration for offering a bid exceeds the day-ahead electricity price and the marginal cost of cycle aging, the EVs actually charge more than necessary to be able to offer a larger bid. This was seen on Day 2, where the EVs, on average, reached a final SoC of 76%, compared with the lower limit of 70%. However, for Day 3, the higher cycle aging for FCR-D up compared with V2H-G is not caused by a higher average end SoC of the EVs. Instead, the fleet of EVs charged with a slightly higher power during hour 20, to be able to increase the bid for that specific hour. As a result, the EVs were able to discharge more energy to the households during hour 5 the following day when the remuneration for offering the bid for FCR-D up was lower than during hour 20. This yielded a higher battery throughput and hence a higher cycle aging cost. The effect is also seen in the calendar aging, where FCR-D has a higher cost compared with V2H. This was caused by the slightly higher average SoC, leading to a faster battery degradation due to the calendar aging.

6
Conclusion

This thesis aimed at evaluating the benefit of utilizing bidirectional charging in electric vehicles (EVs), while considering battery degradation models. Firstly, battery degradation was investigated based on an equivalent circuit model (ECM). The calendar aging and cycle aging were identified. To reduce computational complexity, a bucket model (BM) was fitted based on the ECM.

Then, the battery degradation models were utilized in a vehicle-to-home (V2H) application, where the EV was used as an energy repository for a single household. By utilizing the EV battery as energy storage, the household energy consumption was shifted, which reduced the overall energy cost. Furthermore, the results showed that the calendar aging effect was reduced in V2H compared with uncontrolled charging and smart charging. Additionally, a lower marginal cost arising from battery degradation was observed with a more heavily used EV battery.

Furthermore, it was demonstrated that the V2H optimization problem can be formulated using the BM while still obtaining similar results as the more complex ECM. This improved the computational speed, which is necessary for large-scale applications.

Another vital part of a V2H implementation is the presence of a household energy forecasting model. To illustrate the concept, a simple long short-term memory (LSTM) based forecasting model was constructed based on real household energy consumption data.

Lastly, the V2H application was extended to an aggregated fleet of EVs in a vehicle-to-grid (V2G) setting, where the ability to participate in the frequency regulation markets was investigated. Frequency containment reserve products for both normal and disturbed operation (FCR-N and FCR-D up) showed great profitability potential for the aggregator. FCR-D up emerged as the most profitable product to offer under the investigated days and is also considered to be the easiest to implement in a real-world implementation, due to its nature of rare and short bursts of activation.

7
Future Work

The two battery degradation models presented in this thesis are of different complexities. The one used in the ECM is more comprehensive and uses more variables, such as ΔDoD and the voltage of the battery. By making several assumptions regarding the variables, it was possible to derive a simpler degradation model, which was done for the BM. The simpler degradation model has many advantages in terms of computational cost, as the problem can be solved using linear programming. The results presented in this thesis also showed that the simpler degradation model yields similar results to the more complex one, and hence motivates the use of the simpler degradation model in cases where having a low computational complexity is of high value. Such applications could include scheduling charging of large fleets of vehicles.

However, the more complex degradation model is more likely to reflect the true degradation of the battery and is hence better suited for more detailed charging control of individual vehicles. This motivates the development of an iterative approach, where the more accurate degradation model is used for individual vehicles, which then shares information with a central scheduler that can establish a simple linear degradation model that is used when scheduling the whole fleet.

The problem specified for the V2G case offering frequency regulation through FCR includes V2H on a global scale, meaning that energy from an EV connected to one household can dispatch energy to another household. This was a simplification made. However, in a real-world solution, the structure would preferably consist of a local, more complex, computation that communicates with a cloud computer, corresponding to the aggregator, that aggregates all local computations to one solution, from which the aggregator chooses to offer bids for frequency regulation to the TSO. In short, the problem would be set up as

1. Local computation
    - Set up a strategy for local V2H.
    - Consider: Household energy forecast, cost of battery degradation, EV charging needs, possibly including energy production from a photovoltaic system.
    - Send to the cloud: Optimal charging/discharging profile and the marginal cost of battery degradation per kWh throughput.

2. Cloud computation
    - Set up a strategy for offering frequency regulation bids.
    - Consider: The aggregated optimal charging/discharging profiles of all EVs in the pool to calculate the bid size for each hour, and uncertainty regarding activation level and duration.
    - Send to TSO: Bid size for offered frequency regulation service.
    - Throughout the day: Distribute the necessary activation due to frequency deviations among the participating EVs. Consider: Cost of battery degradation, and lost opportunity cost for carrying out local V2H. Combine both these factors to minimize the reimbursements from the aggregator to the participants.

Another suggestion for future work would be to focus on creating an accurate household energy consumption forecasting model for a single household. Due to time constraints, a minimal amount of time was spent on developing the model in this thesis. However, it would be interesting to investigate how accurate a prediction model could become for a single household.

One last suggestion is to develop a more robust strategy for offering frequency regulation services, without knowledge of future activation or prices. This could be to restrict how many hours in a row the aggregator is able to bid, to ensure recovery time, or to use a lot of historical data to set up a stochastic optimization problem to ensure that the aggregator can fulfill its bids even in the worst-case scenarios.

Bibliography

[1] International Energy Agency. (2019). "Electricity," [Online]. Available: https://www.iea.org/fuels-and-technologies/electricity (visited on Apr. 14, 2022).

[2] L. Paoli and T. Gül. (2022). "Electric cars fend off supply challenges to more than double global sales," [Online]. Available: https://www.iea.org/commentaries/electric-cars-fend-off-supply-challenges-to-more-than-double-global-sales (visited on Apr. 14, 2022).

[3] W. Kempton, J. Tomic, S. Letendre, A. Brooks, and T. Lipman, "Vehicle-to-Grid Power: Battery, Hybrid, and Fuel Cell Vehicles as Resources for Distributed Electric Power in California," 2001. [Online]. Available: https://escholarship.org/uc/item/5cc9g0jp (visited on Feb. 21, 2022).

[4] J. Schmalstieg, S. Käbitz, M. Ecker, and D. U. Sauer, "A holistic aging model for Li(NiMnCo)O2 based 18650 lithium-ion batteries," *Journal of Power Sources*, vol. 257, pp. 325–334, 2014, ISSN: 0378-7753. DOI: https://doi.org/10.1016/j.jpowsour.2014.02.012.

[5] A. Thingvad and M. Marinelli, "Influence of V2G Frequency Services and Driving on Electric Vehicles Battery Degradation in the Nordic Countries," English, in *Proceedings of EVS 31 & EVTeC 2018.*, 31st International Electric Vehicles Symposium & Exhibition & International Electric Vehicle Technology Conference 2018, EVS31 and EVTeC2018 ; Conference date: 30-09-2018 Through 03-10-2018, 2019.

[6] T. Kataria, "Modelling of vehicle to grid interaction," M.S. thesis, Chalmers University of Technology, Institution for Electrical Engineering, 2018. [Online]. Available: https://hdl.handle.net/20.500.12380/256589.

[7] S. I. Vagropoulos and A. G. Bakirtzis, "Optimal bidding strategy for electric vehicle aggregators in electricity markets," *IEEE Transactions on Power Systems*, vol. 28, no. 4, pp. 4031–4041, 2013. DOI: 10.1109/TPWRS.2013.2274673.

[8] J. Dalton, "Optimal Day-Ahead Scheduling and Bidding Strategy of Risk-Averse Electric Vehicle Aggregator : A Case Study of the Nordic Energy and Frequency Containment Reserve Markets," M.S. thesis, KTH, School of Electrical Engineering and Computer Science (EECS), 2018.

[9] P. Lazzeroni, S. Olivero, M. Repetto, F. Stirano, and M. Vallet, "Optimal battery management for vehicle-to-home and vehicle-to-grid operations in a residential case study," *Energy*, vol. 175, pp. 704–721, 2019, ISSN: 0360-5442. DOI: https://doi.org/10.1016/j.energy.2019.03.113.

[10] J. Chen, Y. Zhang, X. Li, B. Sun, Q. Liao, Y. Tao, and Z. Wang, "Strategic integration of vehicle-to-home system with home distributed photovoltaic

power generation in shanghai," *Applied Energy*, vol. 263, p. 114 603, 2020, ISSN: 0306-2619. DOI: https://doi.org/10.1016/j.apenergy.2020.114603.

[11] J. Miller. (2020). "Electric car costs to remain higher than traditional engines," [Online]. Available: https://www.ft.com/content/a7e58ce7-4fab-424a-b1fa-f833ce948cb7 (visited on May 24, 2022).

[12] S. Matz, P. Burda, J. Fuchs, L. Horlbeck, R. Eckl, and M. Lienkamp, "Beschreibung der Modellierungsart sowie der Modellierungsparameter von Elektrofahrzeugen in der Konzeptphase," Mar. 2014. [Online]. Available: https://www.researchgate.net/publication/261174335_Beschreibung_der_Modellierungsart_sowie_der_Modellierungsparameter_von_Elektrofahrzeugen_in_der_Konzeptphase (visited on May 24, 2022).

[13] E. Chemali, M. Preindl, P. Malysz, and A. Emadi, "Electrochemical and electrostatic energy storage and management systems for electric drive vehicles: State-of-the-art review and future trends," *IEEE Journal of Emerging and Selected Topics in Power Electronics*, vol. 4, no. 3, pp. 1117–1134, 2016. DOI: 10.1109/JESTPE.2016.2566583.

[14] G. L. Plett, *Battery Modeling*. Norwood, MA, USA: Artech House, 2015.

[15] B. Pollet, I. Staffell, J. Shang, and V. Molkov, "22 - fuel-cell (hydrogen) electric hybrid vehicles," in *Alternative Fuels and Advanced Vehicle Technologies for Improved Environmental Performance*, R. Folkson, Ed., Woodhead Publishing, 2014, pp. 685–735, ISBN: 978-0-85709-522-0. DOI: https://doi.org/10.1533/9780857097422.3.685.

[16] B. P. Miller, "Automotive lithium-ion batteries," *Johnson Matthey Technology Review*, vol. 59, no. 1, pp. 4–13, Jan. 1, 2015, ISSN: 2056-5135. DOI: doi:10.1595/205651315X685445.

[17] J. B. Goodenough and K.-S. Park, "The li-ion rechargeable battery: A perspective," *Journal of the American Chemical Society*, vol. 135, no. 4, pp. 1167–1176, 2013, PMID: 23294028. DOI: 10.1021/ja3091438.

[18] R. Deshpande, M. Verbrugge, Y.-T. Cheng, J. Wang, and P. Liu, "Battery Cycle Life Prediction with Coupled Chemical Degradation and Fatigue Mechanics," *Journal of The Electrochemical Society*, vol. 159, no. 10, A1730–A1738, 2012. DOI: 10.1149/2.049210jes.

[19] P. Keil, S. F. Schuster, J. Wilhelm, J. Travi, A. Hauser, R. C. Karl, and A. Jossen, "Calendar aging of lithium-ion batteries," *Journal of The Electrochemical Society*, vol. 163, no. 9, A1872–A1880, 2016. DOI: 10.1149/2.0411609jes.

[20] Swissgrid. (2022). "Frequency," [Online]. Available: https://www.swissgrid.ch/en/home/operation/regulation/frequency.html (visited on Feb. 25, 2022).

[21] National Grid ESO. (2022). "What is Frequency?" [Online]. Available: https://www.nationalgrideso.com/electricity-explained/how-do-we-balance-grid/what-frequency (visited on May 5, 2022).

[22] ENTSO-E. (2019). "First milestone of Future Synchronous Connection of the Baltic Power System with Continental Europe," [Online]. Available: https://www.entsoe.eu/news/2019/05/29/first-milestone-of-future-synchronous-connection-of-the-baltic-power-system-with-continental-europe/ (visited on May 17, 2022).

[23] ENTSO-E. (2022). "System Operations Committee," [Online]. Available: https://www.entsoe.eu/about/system-operations/#regional-groups (visited on May 17, 2022).

[24] Svenska Kraftnät. (2022). "Information about ancillary services," [Online]. Available: https://www.svk.se/en/stakeholder-portal/electricity-market/information-about-ancillary-services/ (visited on Feb. 21, 2022).

[25] Energimarknadsinspektionen. (2021). "Hur bör rollen som oberoende aggregator genomföras i Sverige?" [Online]. Available: https://www.ei.se/bransch/flexibilitet-i-energisystemen/kundens-bidrag-till-efterfrageflexibilitet/oberoende-aggregatorer (visited on May 29, 2022).

[26] Svenska Krafnät. (2021). "Prequalification," [Online]. Available: https://www.svk.se/en/stakeholder-portal/Electricity-market/information-about-ancillary-services/prequalification/ (visited on May 29, 2022).

[27] Svenska Kraftnät. (2021). "Frekvenshållningsreserv normaldrift (FCR-N)," [Online]. Available: https://www.svk.se/aktorsportalen/systemdrift-elmarknad/information-om-stodtjanster/fcr-n/ (visited on May 8, 2022).

[28] Svenska Kraftnät. (2021). "Frekvenshållningsreserv störning nedreglering (FCR-D ned)," [Online]. Available: https://www.svk.se/aktorsportalen/systemdrift-elmarknad/information-om-stodtjanster/fcr-d-ned/ (visited on May 9, 2022).

[29] Svenska Kraftnät. (2021). "Frekvenshållningsreserv störning uppreglering (FCR-D upp)," [Online]. Available: https://www.svk.se/aktorsportalen/systemdrift-elmarknad/information-om-stodtjanster/fcr-d-upp/ (visited on May 8, 2022).

[30] Fingrid. (2020). "Frequency quality analysis 2020," [Online]. Available: https://www.fingrid.fi/globalassets/dokumentit/fi/kantaverkko/suomen-sahkojarjestelma/frequency_quality_analysis_2020.pdf (visited on May 17, 2022).

[31] Svenska Krafnät. (2022). "Villkor för FCR," [Online]. Available: https://www.svk.se/siteassets/4.aktorsportalen/systemdrift-o-elmarknad/balansansvar/aktuella-balansansvarsavtal/4620_3-bilaga-3-fcr.pdf (visited on May 29, 2022).

[32] Fingrid. (2022). "Balancing energy and balancing capacity markets," [Online]. Available: https://www.fingrid.fi/en/electricity-market/reserves_and_balancing/balancing-energy-and-balancing-capacity-markets/?fbclid=IwAR2eidcl7pllv9xMQ-nE177d-rhzI_2LF5ZguVf6EZwDgk30OksVh4SRtHo#balancing-energy-pricing (visited on May 29, 2022).

[33] J. M. Reniers, G. Mulder, S. Ober-Blöbaum, and D. A. Howey, "Improving optimal control of grid-connected lithium-ion batteries through more accurate battery and degradation modelling," *Journal of Power Sources*, vol. 379, pp. 91–102, 2018, ISSN: 0378-7753. DOI: https://doi.org/10.1016/j.jpowsour.2018.01.004.

[34] M. Ecker, N. Nieto, S. Käbitz, J. Schmalstieg, H. Blanke, A. Warnecke, and D. U. Sauer, "Calendar and cycle life study of Li(NiMnCo)O2-based 18650 lithium-ion batteries," *Journal of Power Sources*, vol. 248, pp. 839–851, 2014, ISSN: 0378-7753. DOI: https://doi.org/10.1016/j.jpowsour.2013.09.143.

[35] J. Engels, B. Claessens, and G. Deconinck, "Techno-economic analysis and optimal control of battery storage for frequency control services, applied to the german market," *Applied Energy*, vol. 242, pp. 1036–1049, 2019, ISSN: 0306-2619. DOI: https://doi.org/10.1016/j.apenergy.2019.03.128.

[36] W. E. Hart, J.-P. Watson, and D. L. Woodruff, "Pyomo: modeling and solving mathematical programs in Python," *Mathematical Programming Computation*, vol. 3, no. 3, pp. 219–260, 2011.

[37] M. L. Bynum, G. A. Hackebeil, W. E. Hart, C. D. Laird, B. L. Nicholson, J. D. Siirola, J.-P. Watson, and D. L. Woodruff, *Pyomo–optimization modeling in python*, Third. Springer Science & Business Media, 2021, vol. 67.

[38] A. Wächter and L. T. Biegler, "On the implementation of an interior-point filter line-search algorithm for large-scale nonlinear programming," *Mathematical Programming*, vol. 106, no. 1, pp. 25–57, Mar. 2006, ISSN: 1436-4646. DOI: 10.1007/s10107-004-0559-y.

[39] Polestar. (2022). "The car's certified values for range and electricity consumption," [Online]. Available: https://www.polestar.com/uk/manual/polestar-2/2022/article/The-car's-certified-values-for-range-and-electricity-consumption/ (visited on Apr. 25, 2022).

[40] W. Schram, N. Brinkel, G. Smink, T. van Wijk, and W. van Sark, "Empirical Evaluation of V2G Round-trip Efficiency," in *2020 International Conference on Smart Energy Systems and Technologies (SEST)*, 2020, pp. 1–6. DOI: 10.1109/SEST48500.2020.9203459.

[41] Statista. (2021). "Lithium-ion battery pack costs worldwide between 2011 and 2030," [Online]. Available: https://www.statista.com/statistics/883118/global-lithium-ion-battery-pack-costs/ (visited on May 24, 2022).

[42] Trafikanalys. (2021). "Körsträckor 2021," [Online]. Available: https://www.trafa.se/globalassets/statistik/vagtrafik/korstrackor/2021/korstrackor-2021.pdf (visited on Apr. 14, 2022).

[43] Brownlee, Jason. (2018). "Multi-Step LSTM Time Series Forecasting Models for Power Usage," [Online]. Available: https://machinelearningmastery.com/how-to-develop-lstm-models-for-multi-step-time-series-forecasting-of-household-power-consumption/ (visited on Apr. 26, 2022).

[44] Nord Pool. (2022). "Day-ahead prices," [Online]. Available: https://www.nordpoolgroup.com/en/Market-data1/Dayahead/Area-Prices/SE/Hourly/?view=table (visited on May 23, 2022).

[45] Gurobi Optimization, LLC, *Gurobi Optimizer Reference Manual*, 2022. [Online]. Available: https://www.gurobi.com.

[46] Nord Pool. (2022). "Regulating prices," [Online]. Available: https://www.nordpoolgroup.com/en/Market-data1/Regulating-Power1/Regulating-Prices1/SE/Hourly/?view=table (visited on May 23, 2022).

[47] Svenska Kraftnät. (2022). "Primärreglering," [Online]. Available: https://mimer.svk.se/PrimaryRegulation/PrimaryRegulationIndex (visited on May 23, 2022).

[48] Fingrid. (2022). "Download datasets," [Online]. Available: https://data.fingrid.fi/open-data-forms/search/en/ (visited on May 23, 2022).

A

Appendix

Table A.1: Comparisons of user scenarios in the ECM, actual household energy consumption.

		Energy cost [SEK]	Cyc. cost [SEK]	Cal. cost [SEK]	Total [SEK]	Savings
User 1	UC	7,338	168	1,383	8,889	-
	SC	6,967	186	1,364	8,517	4.2%
	V2H	5,592	739	1,347	7,678	16.2%
User 2	UC	7,338	92	1,039	8,469	-
	SC	6,967	102	1,025	8,094	4.4%
	V2H	5,386	677	1,008	7,071	19.1%
User 3	UC	7,338	60	837	8,235	-
	SC	6,967	66	825	7,858	4.6%
	V2H	5,233	615	808	6,656	21.8%
User 4	UC	8,655	307	1,382	10,344	-
	SC	7,527	388	1,330	9,245	10.6%
	V2H	6,011	900	1,305	8,216	22.7%
User 5	UC	8,655	169	1,038	9,862	-
	SC	7,527	213	999	8,739	11.4%
	V2H	5,826	727	976	7,529	25.8%
User 6	UC	8,655	109	836	9,600	-
	SC	7,527	137	804	8,468	11.8%
	V2H	5,669	629	782	7,080	28.4%
User 7	UC	13,181	802	1,369	15,352	-
	SC	9,464	1,077	1,227	11,768	23.3%
	V2H	8,154	1,329	1,188	10,671	32.3%
User 8	UC	13,181	440	1,029	14,650	-
	SC	9,464	590	922	10,976	25.1%
	V2H	7,940	952	885	9,777	35.2%
User 9	UC	13,181	284	828	14,293	-
	SC	9,464	381	742	10,587	25.9%
	V2H	7,797	751	706	9,254	37.2%

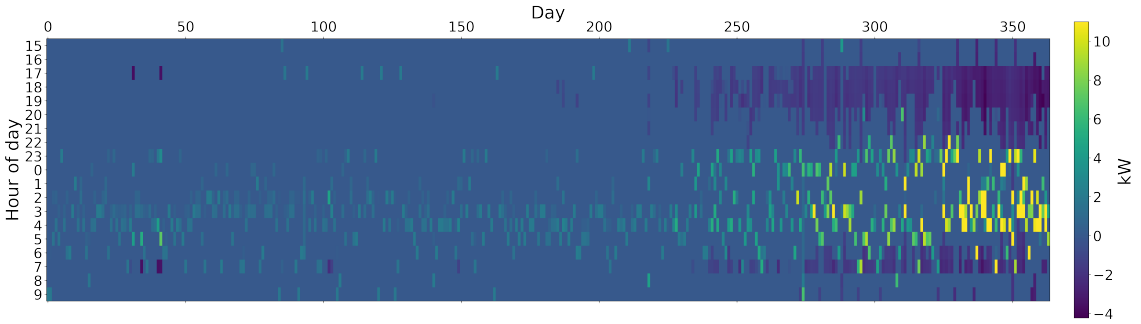

(a) User 1

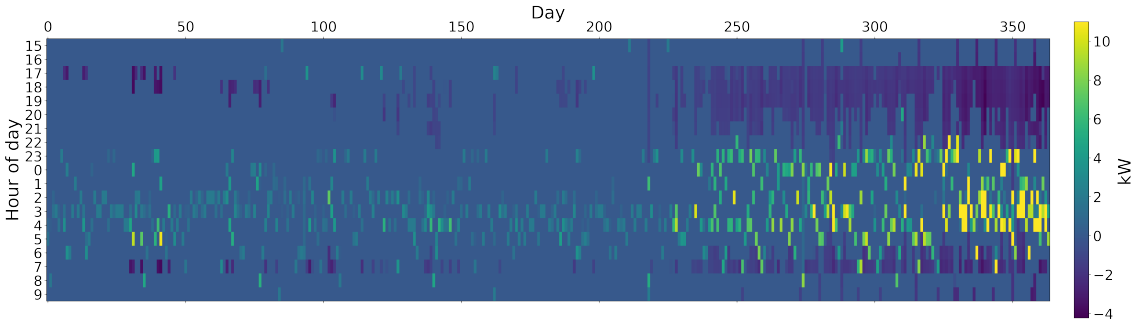

(b) User 2

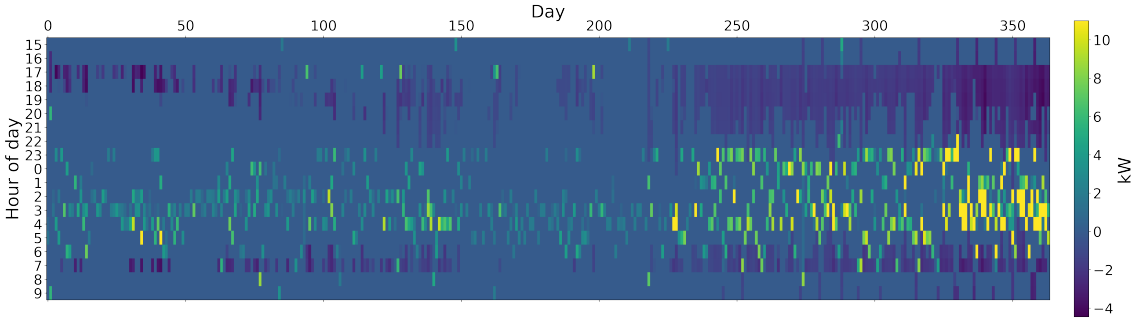

(c) User 3

Figure A.1: V2H charging power as seen from the wallbox, short-distance drivers.

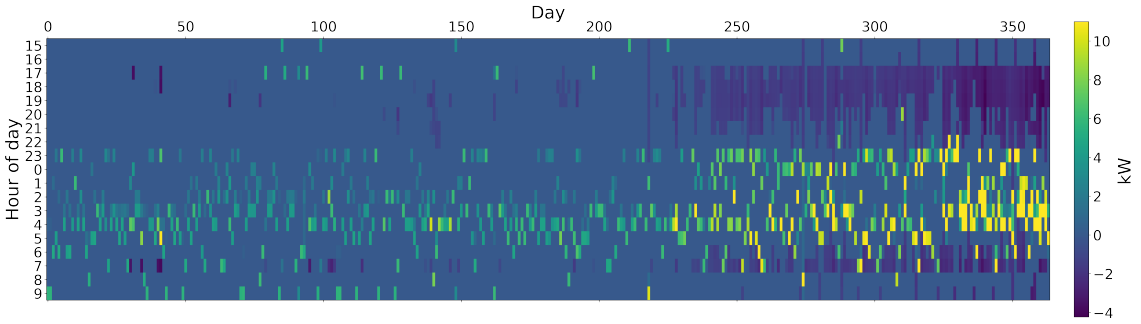

(a) User 4

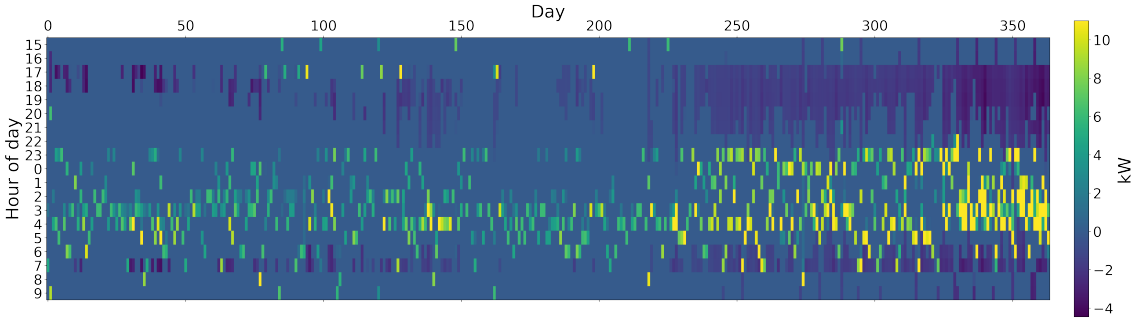

(b) User 5

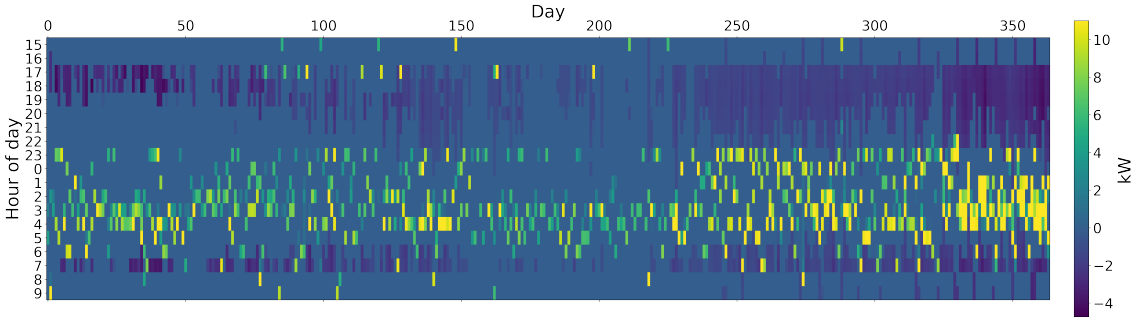

(c) User 6

Figure A.2: V2H charging power as seen from the wallbox, average-distance drivers.

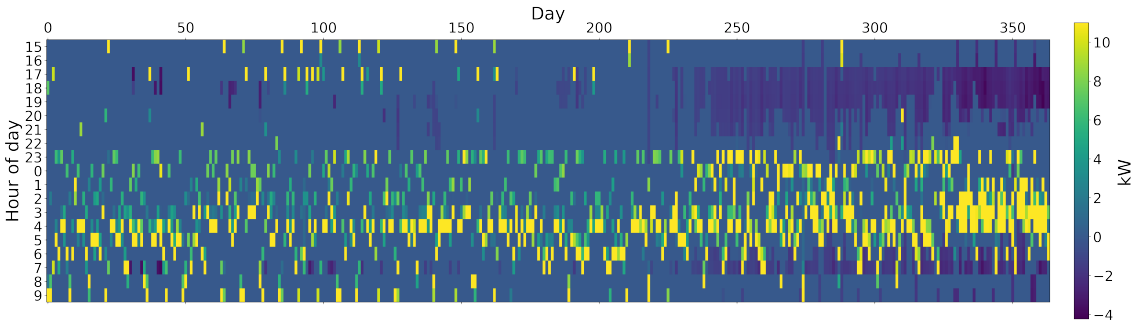

(a) User 7

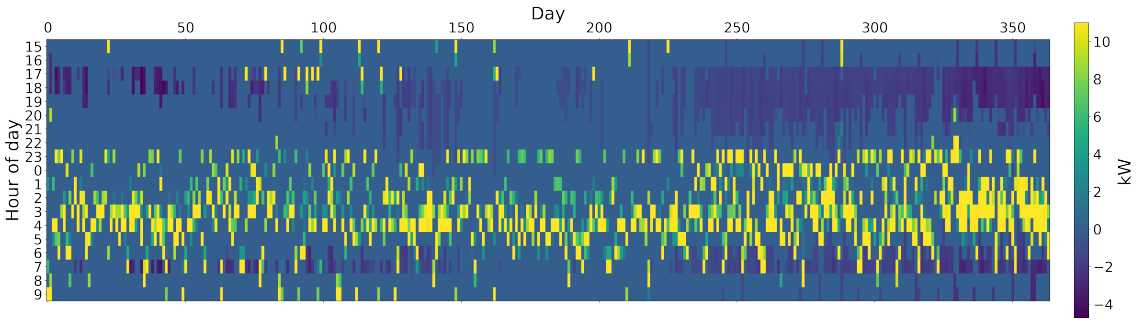

(b) User 8

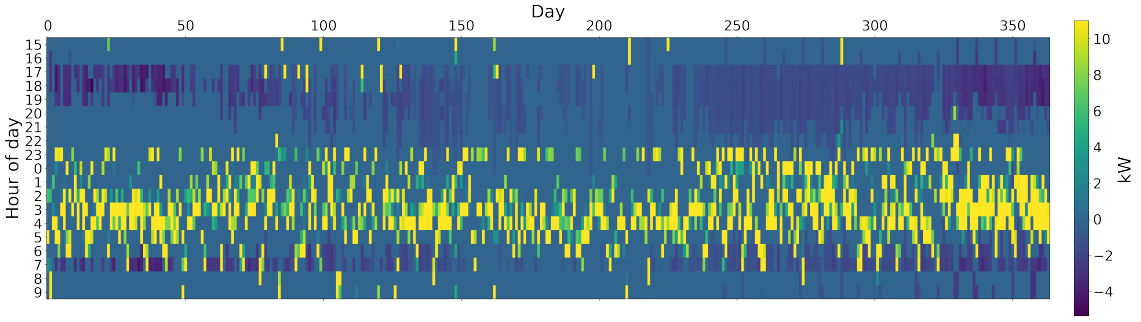

(c) User 9

Figure A.3: V2H charging power as seen from the wallbox, long-distance drivers.

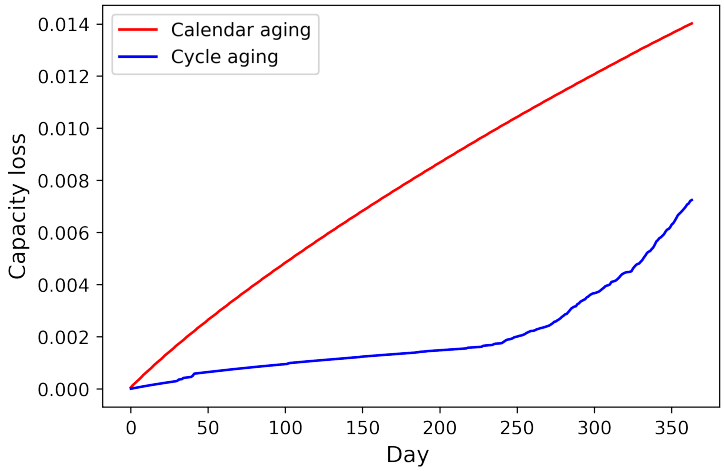

(a) User 1

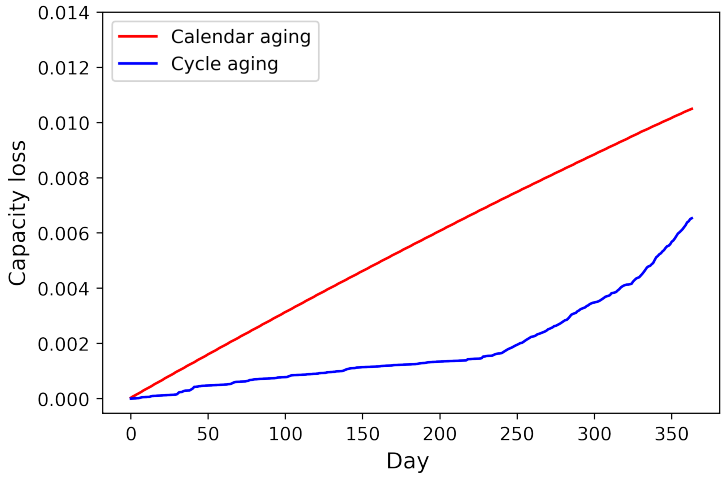

(b) User 2

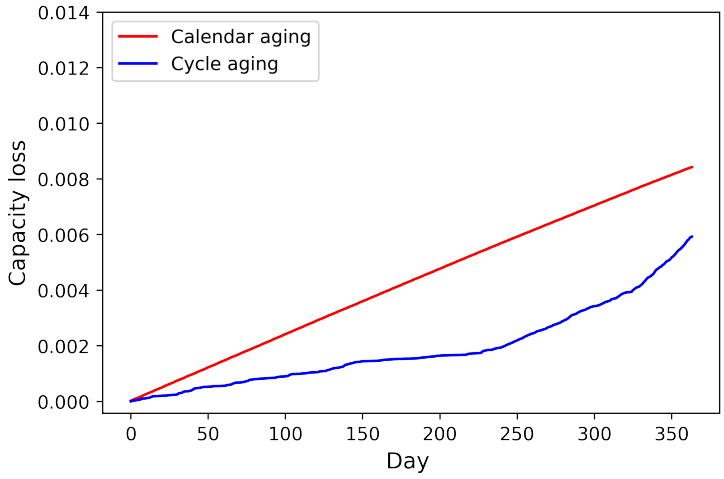

(c) User 3

Figure A.4: Development of normalized capacity loss due to battery aging in V2H, short-distance drivers.

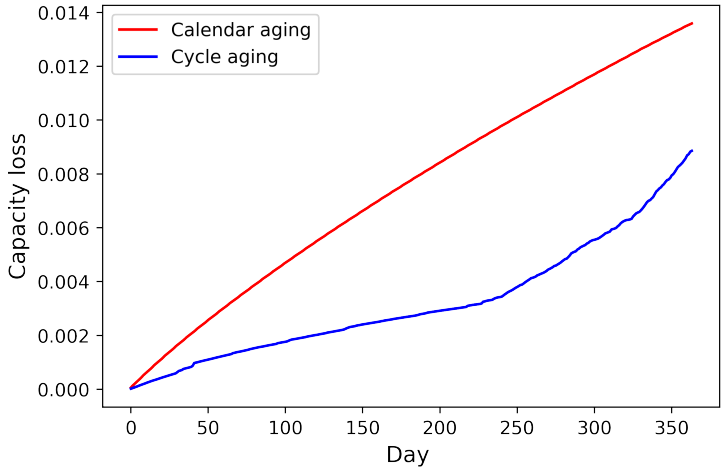

(a) User 4

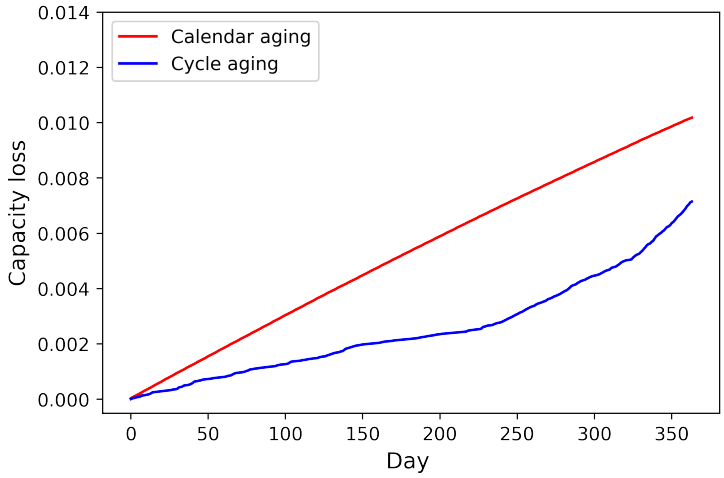

(b) User 5

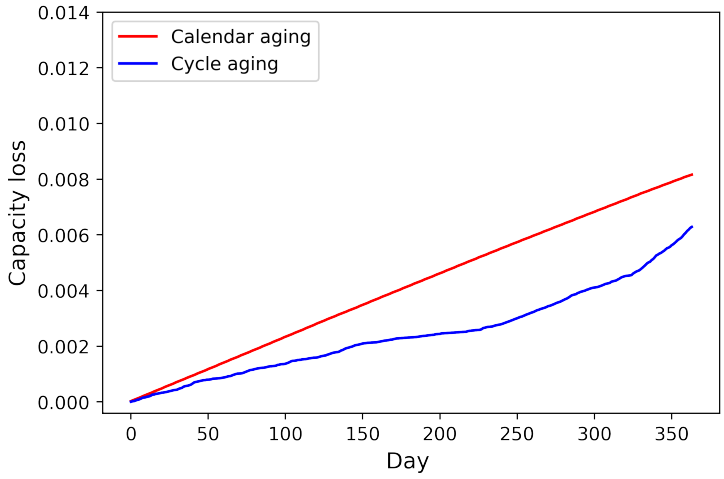

(c) User 6

Figure A.5: Development of normalized capacity loss due to battery aging in V2H, average-distance drivers.

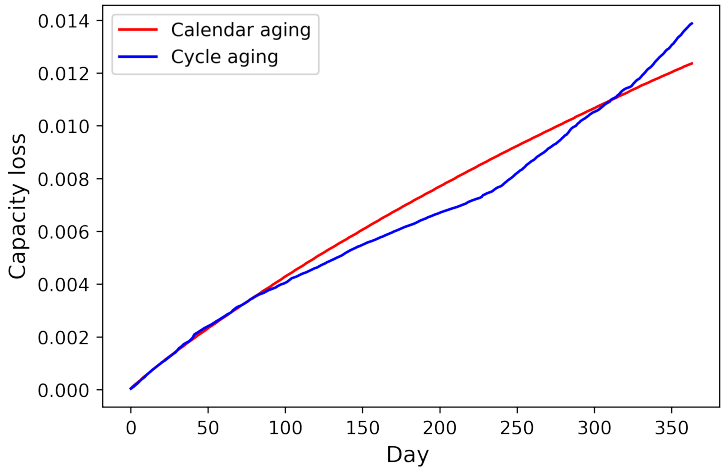

(a) User 7

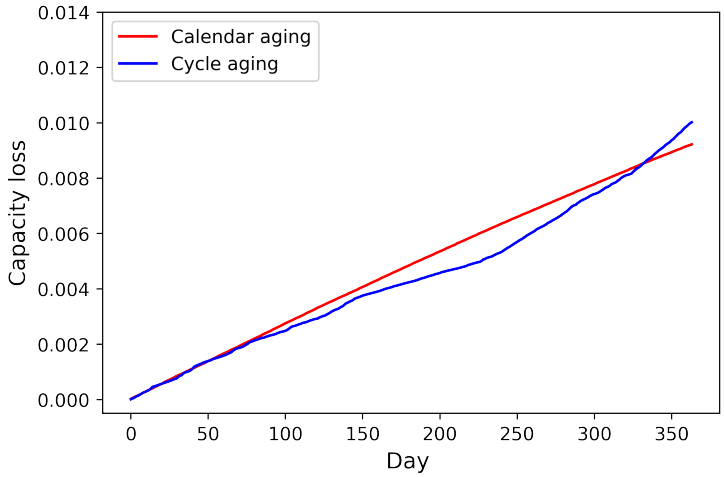

(b) User 8

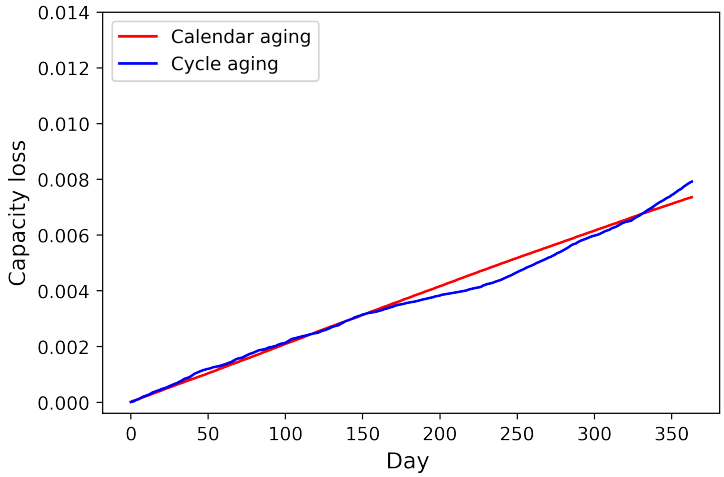

(c) User 9

Figure A.6: Development of normalized capacity loss due to battery aging in V2H, long-distance drivers.

DEPARTMENT OF ELECTRICAL ENGINEERING
CHALMERS UNIVERSITY OF TECHNOLOGY
Gothenburg, Sweden
www.chalmers.se

CHALMERS
UNIVERSITY OF TECHNOLOGY